

## Convection over the Pacific Warm Pool in relation to the Atmospheric Kelvin–Rossby Wave\*

ROBERT A. HOUZE JR.

*Department of Atmospheric Sciences, University of Washington, Seattle, Washington*

SHUYI S. CHEN

*Rosenstiel School of Marine and Atmospheric Sciences, University of Miami, Miami, Florida*

DAVID E. KINGSMILL

*Desert Research Institute, University of Nevada at Reno, Reno, Nevada*

YOLANDE SERRA AND SANDRA E. YUTER

*Department of Atmospheric Sciences, University of Washington, Seattle, Washington*

(Manuscript received 15 February 1999, in final form 18 November 1999)

### ABSTRACT

Deep convection over the western tropical Pacific warm pool is analyzed in terms of its relation to the atmospheric Kelvin–Rossby wave, which dominates the large-scale flow during the austral summer. The study uses Doppler radar data collected by aircraft and ship radars during different time periods in the Tropical Ocean Global Atmosphere Coupled Ocean–Atmosphere Response Experiment to characterize the mesoscale circulations of organized convective cloud systems occurring throughout the season. The study focuses on convection in two contrasting phases of the wave: the “westerly onset region” just west of the point within the wave where low-level easterlies change to westerlies, and the “strong westerly region” (or “westerly wind burst”) lying between the large-scale counterrotating gyres of the Kelvin–Rossby wave.

In the westerly onset region the zonal wind component had midlevel easterlies overlying low-level westerlies. In the strong westerly region a deep layer of westerlies extended from the surface up to the upper troposphere, with a maximum of westerly component at about the 850-mb level. The different vertical shear of the zonal wind in these two regions of the wave led to different momentum transport by the mesoscale circulations that develop into very large “super convective systems” (cloud tops colder than  $-65^{\circ}\text{C}$  over regions of  $\sim 300$  km or more in lateral dimension). The super convective systems developed strong midlevel inflow jets. The direction of the jet was determined by the environmental shear, which in turn was determined by the dynamics of the large-scale wave. In the westerly onset region, the large-scale shear determined that the jet had an easterly component. In the strong westerly region, the jet had a westerly component. In both cases, the inflow intensified within the cloud system as the convective cells of the super convective system filled a broad region with a deep stratiform ice cloud, from which ice particles fell. Evidently, as the particles sublimated and melted, they cooled the air at midlevels in the cloud system. The cooling evidently modified the mesoscale pressure field in the system so as to accelerate the flow of ambient air into the system and to encourage the inflow to subside. In this way, the mesoscale inflow to super convective systems transported easterly momentum downward in the westerly onset region and westerly momentum downward in the strong westerly region, so that the mesoscale momentum feedback of the mesoscale inflow jets were negative in the westerly onset region and positive in the strong westerly region (accelerating the westerly wind burst). These momentum transports by the broad mesoscale midlevel inflow of super convective systems affected broad horizontal regions and were sometimes different in sign from the momentum transports of individual convective-scale cells in the same system.

---

\* Joint Institute for the Study of the Atmosphere and the Oceans Contribution Number 666.

---

Corresponding author address: Professor R. A. Houze Jr., Dept. of Atmospheric Sciences, University of Washington, Box 351640, Seattle, WA 98195-1640.

E-mail: houze@atmos.washington.edu

## 1. Introduction

Over the last 25 years, field projects over the tropical oceans<sup>1</sup> have sought the mechanism of interaction between the large-scale circulation and convective clouds. The problem of the interaction is often broken down into controls and feedbacks. The external controls on convection are the planetary boundary layer thermodynamic state, the potential temperature stratification of the troposphere, the vertical shear of the ambient horizontal wind, the transport of humidity into the large-scale convectively active region, and a triggering mechanism (required to bring parcels of air upward to their level of free convection). All of these controls are features of the synoptic-scale environment, except the triggering, which is a small-scale local concentration of low-level convergence (e.g., a gust front, a land or sea breeze, a convectively induced gravity wave). The small-scale nature of triggering lends a chaotic component to convection; it is intermittent in time and space, only occurring when and where small-scale processes allow it, regardless of large-scale conditions. The convection feeds back to the large-scale dynamics via vertical distribution of heating and momentum transports. In large-scale equations, these feedbacks are often lumped into a bulk heating rate or a momentum source term in a budget equation, or they are expressed in terms of correlations of deviations from a mean or base state. This diagnostic view does not provide insight into the physical *mechanism* of the feedback.

This study focuses on the *phenomenology* of the control–feedback process as a way to gain insight into the physical mechanism of the controls and feedbacks of convective–large-scale interaction over tropical oceans. The data from TOGA COARE (Godfrey et al. 1998) provide an opportunity to understand this phenomenology because the convection was sampled by ship and aircraft Doppler radars over the near-equatorial western Pacific warm pool over a sufficiently long time period (4 months) for the large-scale dynamics to evolve through significantly different stages. The objective of this paper is to combine the radar data with large-scale analysis in such a way as to identify important differences in convective behavior that occur as a function of the large-scale conditions in TOGA COARE. From these differences in radar observations over the 4-month period, we infer aspects of the controls and feedbacks

defining the convective/large-scale interaction over the near-equatorial warm pool.

In analyzing the phenomenology of convective–large-scale interaction over the warm pool, we emphasize two distinctly identifiable phenomena, which seem to be key to understanding the interaction. On the large scale, we emphasize the atmospheric near-equatorial Kelvin–Rossby wave,<sup>2</sup> which dominated the large-scale wind field during much of TOGA COARE (e.g., Chen et al. 1996). In section 3, we will provide some background on the Kelvin–Rossby wave. We have been able to categorize convective events in TOGA COARE in terms of their position within an archetypical Kelvin–Rossby wave. The wave structure defines the large-scale wind environment and hence structure of the convection.

On the smaller scale (compared to the Kelvin–Rossby wave) we emphasize the largest mesoscale convective systems. Using satellite imagery Nakazawa (1988) subjectively identified the largest coherent areas of high cloudiness and found that they moved eastward over the western tropical Pacific. He called these entities “super clusters.” Individual mesoscale cloud clusters within the superclusters moved westward. Mapes and Houze (1993b) tried to make the definition of super clusters more objective by using a tracking algorithm to follow areas of cold cloud tops from one infrared satellite image to the next. Any combination of cloud tops that exhibited continuity for over two days was considered to be a supercluster. In this study we have chosen to use the less restrictive terminology of Chen et al. (1996). They suggested that size alone was important and introduced the concept of a “super convective system,” which was any trackable cloud system that exceeded 300 km in horizontal dimension at any time in its lifetime. The super convective systems appear to be especially significant in relation to interactions with large-scale dynamics. For example, Chen and Houze (1997) found that interannual variability in high cloudiness over the warm pool was accounted for almost entirely by the super convective systems.

In this study, we examine the relationship of observed convective cloud systems to the Kelvin–Rossby wave in TOGA COARE. We find that the velocity fields in super convective systems have important features that are distinct from smaller mesoscale convective systems, and that the momentum feedbacks by the super convective systems depend critically on the ambient large-scale flow regime. Specifically, we will present evidence that the momentum feedbacks by the large organized convective systems may be positive or negative depending on where the cloud systems are located with respect to large-scale wave structure.

---

<sup>1</sup> The Global Atmospheric Research Programme (GARP) Atlantic Tropical Experiment (Kuettner and Parker 1976), the GARP Winter and Summer Monsoon Experiments (Greenfield and Krishnamurti 1979; Fein and Kuettner 1980), the Australian Monsoon Experiment and Equatorial Mesoscale Experiments (Holland et al. 1986; Webster and Houze 1991), the Tropical Ocean Global Atmosphere Coupled Ocean–Atmosphere Response Experiment (TOGA COARE; Godfrey et al. 1998), and the Pan American Climate Studies Tropical Eastern Pacific Process Study (Yuter and Houze 2000).

---

<sup>2</sup> We use the term “Kelvin–Rossby wave” to refer to the combined horizontal and vertical structure of the equatorial Kelvin and Rossby waves.

## 2. Data used in this study

### a. Large-scale wind field and satellite data

We determined the large-scale wind field during TOGA COARE (1 November 1992–February 1993) by analyzing the European Centre for Medium-Range Weather Forecasts (ECMWF) uninitialized global wind analysis fields at 0000 and 1200 UTC. We obtained the pattern of high cloudiness from hourly infrared (IR) satellite images from the Japanese Geosynchronous Meteorological Satellite (GMS), provided by the Australian Bureau of Meteorology, with about 10-km resolution (highest resolution approximately 9 km at the subsatellite point). For further discussion of these datasets see Chen et al. (1996).

### b. Dual-Doppler radar data collected by aircraft

We determined the internal structures of convective cloud systems by analyzing the three-dimensional reflectivity and velocity fields from Doppler radars on specially equipped aircraft and ships. Aircraft missions were conducted on 59 different days in TOGA COARE. Three aircraft were instrumented for X-band dual-Doppler radar measurements: two National Oceanic and Atmospheric Administration (NOAA) WP-3D aircraft (designated N42 and N43) and the National Center for Atmospheric Research (NCAR) Electra aircraft. These radars had a wavelength of 3.2 cm; peak power of 60 kW (N42 and N43) and 35 kW (Electra); and beamwidths of 1.35° horizontal, 1.9° vertical (N42 and N43), and 1.8° horizontal and vertical (Electra). Pulse repetition frequencies of 1600 Hz (N42 and N43) and 2000 Hz (Electra) gave unambiguous velocities of 13 and 16 m s<sup>-1</sup> for the two aircraft, respectively. The data sample obtained by these airborne Doppler radars has been described by Yuter et al. (1995), Hildebrand et al. (1996), Yuter and Houze (1997, 1998), and Kingsmill and Houze (1999a).

An antenna on the tail of each of the three dual-Doppler aircraft scanned a quasi-vertical plane and measured both reflectivity and radial velocity. Each radar operated by alternating scanning between ~20° fore and ~20° aft of the plane orthogonal to the aircraft heading. Since the aircraft moved rapidly, the beams of the fore and aft scans intersected at 40°–45° angles and were temporally offset from each other by ~1 min for each 10 km of perpendicular distance from the aircraft track. The Doppler radial velocity information from these intersecting scans was combined to synthesize three-dimensional wind fields using the Fore–Aft Scanning Technique (FAST) dual-Doppler methodology of Jorgensen et al. (1996).

For selected time periods (156 in all) more or less evenly distributed through all the flights, the fore and aft scans were combined quantitatively to synthesize three-dimensional wind fields. NCAR's RDSS software (Oye and Carbone 1981) was used to unfold aliased

radial velocities into their proper Nyquist interval. The Doppler data collected by the aircraft were interpolated with REORDER (Cressman 1959; Oye et al. 1995) to one of two Cartesian grids, depending upon the radar-scanning strategy. If the radar scanned on both sides of the aircraft, we used a grid 1.5 km × 1.5 km in the horizontal and 0.8 km in the vertical. If the radar scanned on just one side of the aircraft, we used a grid 0.75 km × 0.75 km in the horizontal and 0.8 km in the vertical in order to take advantage of the higher sampling rate in the direction of the aircraft ground track. After interpolation, three-dimensional wind fields were synthesized using the FAST dual-Doppler methodology in the NCAR CEDRIC software package (Mohr et al. 1986). Once the three-dimensional wind fields were derived, we visualized, perused, and qualitatively analyzed the three-dimensional airborne-Doppler-derived wind fields in all 156 analyzed time periods comprehensively with the aid of NCAR's Zebra software (Corbet et al. 1994).

### c. Single-Doppler radar data collected by ships

Two ships in TOGA COARE were equipped with scanning C-band Doppler radars: the *Xiangyanghong #5* and the *Vickers*. The radars were similar with a wavelength of 5 cm, peak power at 250 kW, beamwidth 1.5°, and a pulse repetition frequency of 1000 Hz. The wavelength and pulse repetition frequency led to a maximum unambiguous velocity measurement (Nyquist velocity) of 14 m s<sup>-1</sup>. Other characteristics of these radars are outlined by Short et al. (1997), who discussed precipitation-measuring aspects of the ship radars. In this study we do not use the precipitation-measuring feature of the two radars. Instead, we have made extensive use of the Doppler velocity data collected by the ship radars to reveal the internal dynamics of convective systems occurring over the ship network. The radial velocity data are unfolded in RDSS and interpolated to a three-dimensional grid in REORDER (2 km × 2 km in the horizontal, 1 km in the vertical). As for the aircraft Doppler radar data discussed above, the three-dimensional Cartesian-gridded reflectivity and radial velocity data were visualized, perused, and analyzed in Zebra. Since the two ships were located too far apart to combine their data in a dual-Doppler synthesis, the data had to be analyzed as single-Doppler data. Nevertheless, the radial velocity, when visualized in three dimensions, contained substantial information on the nature of the internal cloud circulations.

## 3. Gill's Kelvin–Rossby wave paradigm and mesoscale organization of convective cloud systems in the tropical atmosphere

Deep convection over the warm pool distributes the heat gained from the ocean surface through a deep layer of the atmosphere, and the dominant large-scale atmospheric response to the heated air column is a

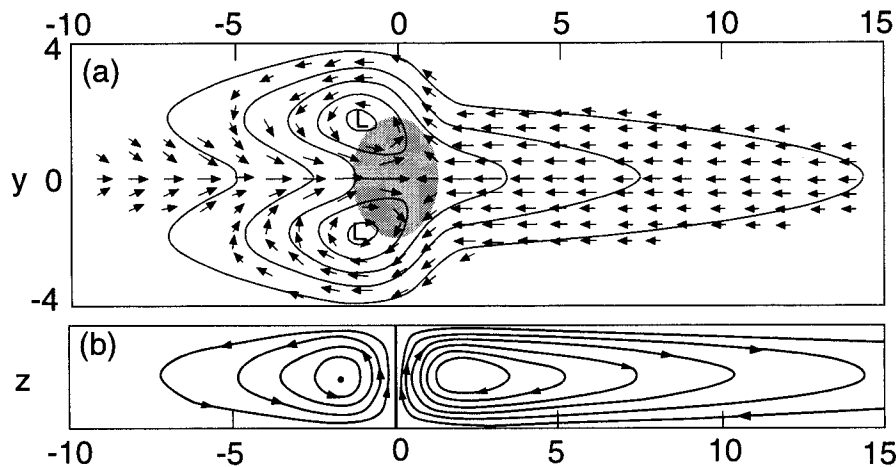


FIG. 1. Zonally asymmetric circulation produced by a deep heating anomaly over the equator (stippled). (a) Plan view of surface motion. (b) Streamlines in a vertical cross section over the equator. (From Gill 1980 as shown by Salby 1996.)

Kelvin–Rossby wave combination (Webster 1972, 1973, 1994; Gill 1980; Lau et al. 1989), which is illustrated in Fig. 1 for an idealized steady-state atmosphere with a heat source at the equator. The Kelvin and Rossby modes combine to produce a zonally asymmetric circulation. Large cyclonic gyres associated with the Rossby waves in the low-level winds lie *symmetrically* on either side of the heat source, with a zone of westerlies lying between the two gyres. If surface friction is included in the idealized calculation, the low-level convergence moves farther east, into the region of mean easterlies (Wang 1988).

The intraseasonal oscillation (ISO), described by Madden and Julian (1971, 1972, 1994), is a slow, somewhat sporadic eastward migration and development of a pattern resembling the idealized steady-state equator-centered wind pattern illustrated in Fig. 1. The ISO occurs over the warm tropical Indian and western Pacific Oceans. The exact relationship of the ISO to atmospheric waves is a matter of debate. However, certain facts are evident from Madden and Julian and from many other studies. The oscillation has a period of 30–60 days. Two episodes of the sporadically moving pattern occurred over the warm pool during December 1992–February 1993.

Figure 2 shows two realizations of the strong westerly phase of the Kelvin–Rossby-like wave during TOGA COARE. These figures show 1-week-average 850-mb wind (computed from the ECMWF wind fields) and the percent high cloudiness (computed from the GMS satellite infrared imagery). These real ISO wind and cloud patterns differ from the idealized Kelvin–Rossby response in Fig. 1 in several respects:

- The westerlies tended to lie off the equator, usually a few degrees south during the austral summer. The coinciding centers of convection and low-level westerlies associated with the ISO have a clear seasonal

shift from north to south of the equator from November to March (e.g., Hendon and Liebmann 1994). This meridional shift has a strong interannual variability (Chen and Houze 1997).

- As noted by Chen et al. (1996), deep convection (and thus the heating) occurred in the region of westerlies, not in the region where the easterlies and westerlies meet (as suggested by Fig. 1) nor in the region of easterlies [as suggested by the calculations of Wang (1988)]. The deep convection was concentrated both in the strong westerly core of the system and in the gyres. Hendon and Salby (1994) also found that the convection extended all the way along the zone of strong low-level westerlies in a composite of ISO life cycle.
- The Kelvin–Rossby structure in these real cases exhibited vertical variability (e.g., sloping interfaces between easterlies and westerlies) that is not part of the idealized structure. This aspect will be discussed further in section 6. These vertical variations may be related to the non-steady-state nature of the real wave structures.

In linear models, the magnitude and vertical scale of the Kelvin–Rossby structure depend on the amplitude, vertical scale, and shape of the vertical profile of the heating, which forces the wave (Chang 1977; Hartmann et al. 1984). The latter study showed that the Kelvin–Rossby response has a more realistic vertical structure if the heating maximum associated with convection is assumed to be in the upper rather than the middle troposphere. That result implies that the steady response is sensitive to the mesoscale organization of the convection; the upward-shifted net heating maximum is more consistent with the structure of observed ensembles of organized mesoscale convective systems, which (in contrast to isolated convective cells) have competing cooling and heating processes at low levels but only

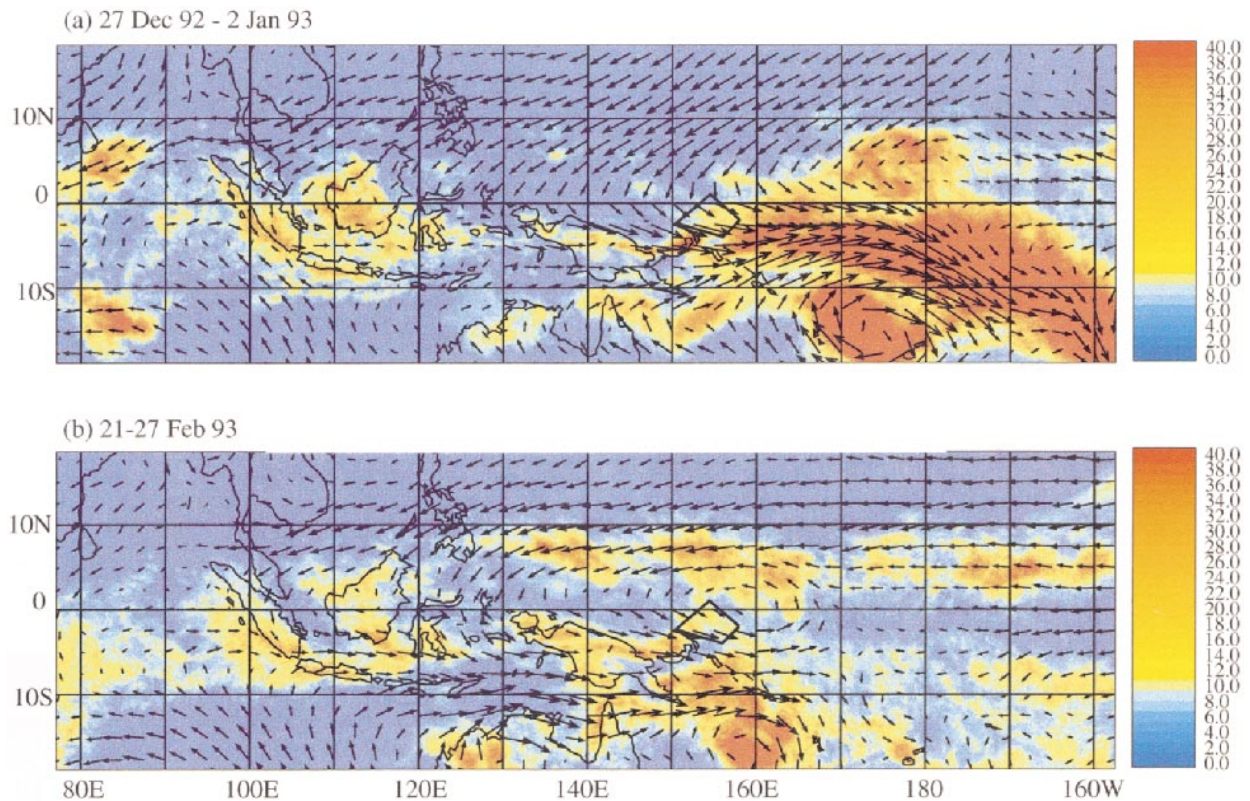


FIG. 2. Weekly percent high cloudiness calculated as a percentage of time during the indicated week that each  $10 \text{ km} \times 10 \text{ km}$  pixel in the GMS IR image had a value of  $235 \text{ K}$  or less. Also shown is the weekly mean wind from the ECMWF global wind analysis at  $850 \text{ mb}$  with  $2.5 \times 2.5$  grid resolution. Wind vectors are scaled such that  $20 \text{ m s}^{-1}$  is represented by a vector that would be  $2.5^\circ$  in length on the map. The TOGA COARE intensive flux array (IFA) is outlined. (From Chen et al. 1996.)

heating processes at mid- to upper levels, thus elevating the large-scale net heating maximum to the upper troposphere (Houze 1982, 1989; Mapes and Houze 1992, 1993a, 1995). These studies thus suggest that the mesoscale organization of the deep convection, that is, the manner in which the deep convection is organized into horizontally extensive complexes with mesoscale circulations and stratiform precipitation regions, is key to understanding convective–large-scale dynamic interaction in the Tropics.<sup>3</sup>

#### 4. Midlevel inflow into mesoscale convective cloud systems—An agent of convective–large-scale dynamic interaction

If the mesoscale organization of convection is a critical factor in the convective–large-scale interaction in the large-scale Kelvin–Rossby wave, the question aris-

es: what aspect (or aspects) of the mesoscale organization is important? In their examination of the aircraft radar observations of mesoscale convective systems in TOGA COARE, Kingsmill and Houze (1999a,b) found that a layer of midlevel air of low equivalent potential temperature ( $\theta_e$ ) always flowed into and toward the center of the mesoscale precipitating cloud systems. Low- $\theta_e$  air in the environment entered the cloud system as subsaturated air and subsided in a layer lying at and just below the sloping base of the precipitating upper cloud shield, under which it was evidently cooled by sublimation and melting of precipitating ice particles, and by evaporation of raindrops when the air sank below the  $0^\circ\text{C}$  level. The large horizontal extent of such midlevel inflows was first noted by Zipser (1969) in studying tropical oceanic convective storms organized into rapidly propagating squall lines. Smull and Houze (1987) discussed the ubiquity of these “rear inflow jets” in squall lines and showed the direct spatial connection between the mesoscale midlevel inflow and the low-level cold pool in the convective region. Analyzing TOGA COARE aircraft data, Kingsmill and Houze (1999a) showed the mesoscale midlevel inflow to be a more general phenomenon than recognized in these previous studies. It is not just a feature of rapidly propa-

<sup>3</sup> The mesoscale organization of convection is also key to understanding the cloud radiative feedbacks in the atmosphere over the warm pool. The radiative transfer is strongly affected by the extensive long-lived upper-level cloud produced by the mesoscale-organized convection.

gating squall line systems; robust midlevel inflows appear to occur in horizontally extensive deep convective systems over the warm pool whether the convective systems are organized into squall lines or not. This midlevel inflow may be thought of as the subsiding branch of the thermally direct *mesoscale* circulation that develops in connection with a mesoscale convective system of the type that dominates warm pool convection. Smull and Houze (1987) noted that while a mesoscale midlevel inflow tends to be generated internally within any individual mesoscale convective system, a few seem to enter the mesoscale system at speeds that are too great to be internally generated. These cases are evidently aided by large-scale dynamics, which determine the wind shear in the storm environment. Zhang and Gao (1989) showed that the midlevel inflow in midlatitude mesoscale convective systems was aided by the baroclinic structure of the midlatitude synoptic-scale wave in which it was occurring. In the TOGA COARE setting, Moncrieff and Klinker's (1997) model results indicate that the super convective systems<sup>4</sup> in the strong westerly phase of the Kelvin–Rossby wave have midlevel inflow controlled by the large-scale dynamic setting and that this midlevel inflow subsides and is a primary agent in the large-scale vertical exchange of mass and momentum.

Since the midlevel inflows are ubiquitous in tropical super convective systems of the TOGA COARE region, have a direct connection with the larger-scale ambient flow, and cover very large areas, we suspect that the midlevel inflows to super convective systems are a key to understanding convective–large-scale process interaction over the warm pool. In this study we therefore examine the behavior of the midlevel mesoscale inflow as a function of the location of the super convective system with respect to the large-scale Kelvin–Rossby wave in which they occur.

### 5. Super convective cloud systems in TOGA COARE in relation to the wind pattern of the observed large-scale Kelvin–Rossby wave

Since the ship and aircraft Doppler-radar observations are our primary source of information on the mesoscale circulations of the deep convective systems in TOGA COARE, we positioned all the mesoscale precipitation systems sampled by ship and aircraft radar (sections 2b, c) with respect to the archetypical Kelvin–Rossby wave. Inspection of the ECMWF global analysis wind fields

<sup>4</sup> Moncrieff and Klinker (1997) defined a “supercluster” conceptually as a conglomerate of several mesoscale convective systems containing still smaller convective-scale cloud elements. This definition emphasizes only size, not duration, and thus corresponds more closely to Chen et al.'s (1996) definition of a super convective system than to previous definitions of a supercluster as a longlasting trackable system.

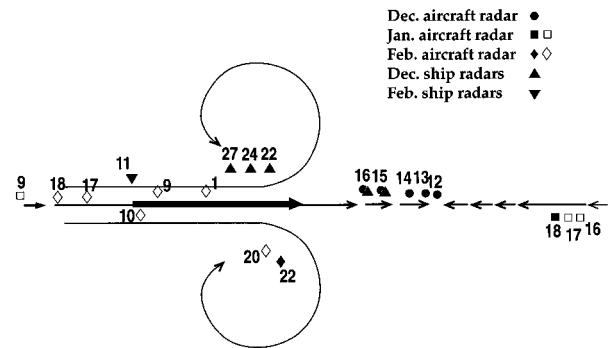


FIG. 3. Locations in relation to the archetypical Kelvin–Rossby wave of ship and aircraft radar data obtained on different days during TOGA COARE. The idealized streamlines are drawn as they would appear on a map of the winds at the 850-mb level. The bold streamline indicates where the winds were strongest. Solid symbols indicate observations of super convective systems. Open symbols indicate smaller mesoscale convective systems, not large enough to meet the criterion of a super convective system. Numbers indicate the day of the month.

over the TOGA COARE domain suggests that from early December 1992 through February 1993, the last three months of TOGA COARE, the winds over the domain had the basic characteristics of a Kelvin–Rossby wave. (For most of November 1992, the first month of TOGA COARE, the large-scale wind patterns were substantially different, having more the character of mixed Rossby–gravity waves.) Figure 3 shows where the ship and aircraft radars sampled mesoscale precipitation systems in relation to the large-scale wave structure. Although this composite was constructed subjectively, the wind patterns were so clear and robust that there is little doubt that the ships and aircraft have been correctly positioned relative to the large-scale wave structure [see Fig. 8 of Chen et al. (1996) for the actual wind patterns seen from week to week over the TOGA COARE domain]. The data samples were well scattered with respect to the large-scale flow pattern. Examined alone, a single case or two of radar data would not present a picture of systematic variation of mesoscale convective systems with respect to the large-scale flow. However, when the data samples are viewed as a group, the ship and aircraft radars (distribution of points in Fig. 3) are seen to have sampled a distribution of mesoscale systems representative of various phases of the planetary-scale Kelvin–Rossby wave. The sampled cloud systems that were large enough to satisfy the Chen et al. (1996) definition of a super convective system are indicated by solid symbols in Fig. 3. Those not meeting definition are plotted as open symbols. The radar data collected on most of these dates have been examined in previously published studies (Table 1).

### 6. Large-scale wind shear in two parts of the Kelvin–Rossby wave

To understand the behavior of the midlevel inflows in relation to the Kelvin–Rossby wave, one requires

TABLE 1. Case studies of TOGA COARE radar data obtained in the Kelvin–Rossby wave regime.

Case	Reference
12 December 1992	Kingsmill and Houze (1999a,b), Yuter and Houze (1998)
13 December 1992	Chong and Bousquet (1999), Kingsmill and Houze (1999a,b), Yuter and Houze (1997, 1998)
14 December 1992	Kingsmill and Houze (1999a,b), Yuter and Houze (1997, 1998)
15 December 1992	Kingsmill and Houze (1999a,b), Yuter and Houze (1997, 1998)
9 February 1993	Hildebrand et al. (1996), Roux (1998), Peterson et al. (1999), Kingsmill and Houze (1999a,b), Yuter and Houze (1997, 1998)
10 February 1993	Kingsmill and Houze (1999a,b), Yuter and Houze (1997, 1998)
11 February 1993	Halverson et al. (1999)
18 February 1993	Hildebrand et al. (1996), Hildebrand (1998), Kingsmill and Houze (1999a,b), Yuter and Houze (1997, 1998)
20 February 1993	Lewis et al. (1998), Kingsmill and Houze (1999a,b), Yuter and Houze (1998)
22 February 1993	Jorgensen et al. (1997), Kingsmill and Houze (1999a,b), Yuter and Houze (1998)

knowledge of both the horizontal and vertical structure of the wind field in the large-scale environment. This paper compares two distinct regions of the wave structure: the “westerly onset region,” the region just to the west of the changeover from easterly to westerly winds (12–16 December in Fig. 3); and the “strong westerly region,” consisting of the westerly jet located between the two gyres of the Kelvin–Rossby wave (22–27 December and 1–11 February in Fig. 3). The strongest part of the westerly region of the Kelvin–Rossby wave is often called the “westerly wind burst.”

The vertical shear was dominated by the zonal component of the wind. Figure 4a displays the zonal component of the wind in the westerly onset region of the Kelvin–Rossby wave. It is a time-mean meridional cross section along 155°E, the longitude of the TOGA COARE intensive flux array (IFA). The composite in Fig. 4a is constructed of the winds observed at the time of the flights of 12–15 December 1992 (dots in Fig. 3). Figure 4b is a similar north–south cross section, in this instance showing the zonal wind in the strong westerly zone of the Kelvin–Rossby wave during the time of the ship radar data collection during 21–27 December 1992 (triangles in Fig. 3). From these composite cross sections, it is evident (as noted in section 3) that the actual

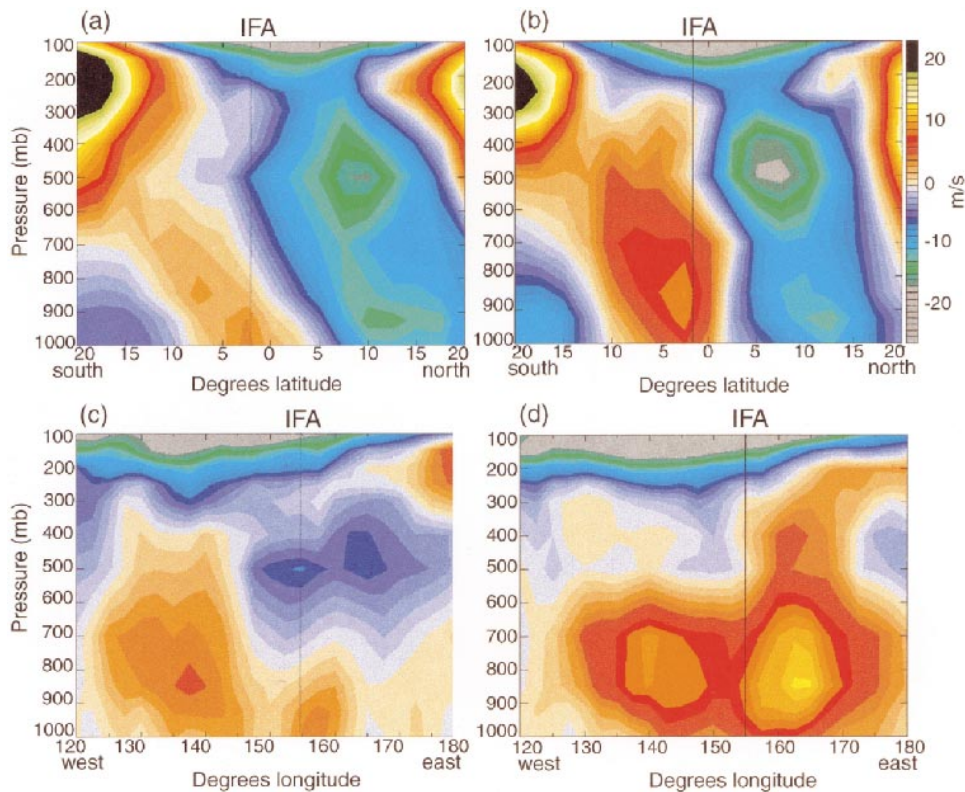


FIG. 4. Time-averaged  $u$ -component of the wind from ECMWF analysis fields along 155°E, the longitude of the TOGA COARE intensive flux array (IFA) for (a) 12–15 Dec 1992 and (b) 21–26 Dec 1992. Time-averaged  $u$  component of the wind from ECMWF analysis fields along 2°S for (c) 12–15 Dec 1992 and (d) 21–26 Dec 1992. The vertical line marks the location of the IFA.

wave pattern in TOGA COARE had vertical structure of a complexity not present in idealized linear models such as that illustrated in Fig. 1.

We included only the late December dates from Fig. 3 in the composite of Fig. 4b because they occurred in the heart of the westerly jet and so they would be most directly comparable with the data from the immediately preceding mid-December westerly onset period shown in Fig. 4a. It is readily confirmed from Fig. 3 of Lin and Johnson (1996) that the vertical shear of the zonal wind in early February was rather similar to that of late December.

In the westerly onset zone (Fig. 4a), the shear was strong at low levels; the wind switched from having a westerly component near the surface to having a strong easterly component in the midtroposphere. In the strong westerly regime (Fig. 4b), the  $u$ -component wind profile showed a jet at about the 850-mb level, and the westerlies extended through a deep layer. The difference in the vertical shear of the  $u$ -component wind seen at the latitude of the IFA in Fig. 4a compared to Fig. 4b is of particular importance to the convective-large-scale interaction. Figures 4c,d show composite zonal sections along  $2^{\circ}\text{S}$  for the same times as Figs. 4a,b, respectively.

The difference in large-scale shear between the westerly onset region and the strong westerly core of the Kelvin-Rossby wave (cf. Fig. 4a and 4b) suggests that the mesoscale-convective dynamics, and hence probably also the convective-large-scale interaction, could be fundamentally different in the westerly onset and strong westerly subregions of the wave complex. It is well known that environmental shear has a pronounced organizing effect on deep convection (Weisman and Klemp 1984, 1986; Rotunno et al. 1988; Weisman et al. 1988; Houze et al. 1990; Skamarock et al. 1994). Over the equatorial oceans the thermodynamic stratification is rather uniform. Though the air is often unstable, the stratification never deviates much from moist adiabatic with a value of moist static energy determined by the temperature of the underlying sea surface (Betts 1974; Xu and Emanuel 1989; Raymond 1995; Kingsmill and Houze 1999b). Since over the warm pool the sea surface temperature varies only slightly, the atmospheric temperature stratification does not vary greatly, and the environmental wind shear and humidity stratification must be the primary determinants of the types of circulations developing within convective systems. Mapes and Zuidema (1996) and Johnson and Lin (1997) have investigated aspects of the humidity field in relation to TOGA COARE convection. In this paper we focus on the role of the large-scale wind shear.

The environmental shear affects the vorticity and pressure fields within individual convective cells and hence the manner in which updrafts redevelop (Weisman and Klemp 1984, 1986). The environmental shear also determines whether convective cells will tend to arrange in lines (Rotunno et al. 1988; Weisman et al. 1988). Sustaining a line or group of convective cells is an es-

sential step toward the convection becoming organized upscale into a larger, longer-lived disturbance, with more widespread gust fronts. A sheared environment furthermore favors the formation of a stratiform precipitation region by distributing the upper portions of weakening convective updrafts and ice particles over a broad region of the storm (Houze et al. 1989; Fovell and Ogura 1988, 1989; Houze 1993; Yang and Houze 1995). The formation of the stratiform precipitation region is another important step in the organization of the deep convection into a larger mesoscale disturbance. As the stratiform precipitation region grows, organized mesoscale circulation and broad precipitating upper-level cloud develop (Zhang and Fritsch 1987, 1988a,b; Chen and Frank 1993). The development of this upper-level cloud allows microphysical feedbacks to the large-scale flow, specifically cooling by sublimation, melting, and evaporation, to be spread over a mesoscale (as opposed to convective scale) region. The development of the upper-level cloud deck also affects the radiative feedbacks to the dynamics (Webster and Stephens 1980; Houze 1982).

Since the convective cloud dynamics and the ability of convection to organize into mesoscale convective systems are strongly affected by the large-scale wind field and its variation with height, we a priori expect a relationship to exist between the large-scale shear and the organization of deep convection into mesoscale systems in the TOGA COARE regime. This expectation is further raised by the behavior of the surface wind and temperature at the IMET buoy ( $1.75^{\circ}\text{S}$ ,  $156^{\circ}\text{E}$ ) in the IFA. The IMET buoy data for December 1992 (Fig. 5) show a fairly constant sea surface temperature throughout the month. The surface air temperatures show large departures, with air several degrees colder than the ocean obtaining over periods of a few hours to 1–2 days. These departures are directly associated with the passage of super convective systems characterized by rainfall and cold cloud tops in satellite IR imagery. Figure 6b and 6c show a group of mesoscale convective systems compose a super convective system moving east to west over the IFA and passing over the buoy between 1100 and 1800 UTC on 11 December 1992. Figure 5 shows that this passage corresponded to a drop in air temperature and an easterly peak in the  $u$  component of the wind. During the westerly onset phase of the Kelvin-Rossby wave, the buoy consistently showed mesoscale cold air temperature departures accompanied by the appearance of easterlies or, at least, a *decrease* of westerly wind (Fig. 5a). During the strong westerly phase (Fig. 5b), the cold air temperature episodes tended to be accompanied by an *increase* in the strength of the westerly wind component. This behavior suggests that during the strong westerly phase, momentum transports by super convective systems systematically increased the low-level westerlies [consistent with the model results of Moncrieff and Klinker (1997)] but that during the westerly onset phase of the Kelvin-Rossby wave the me-

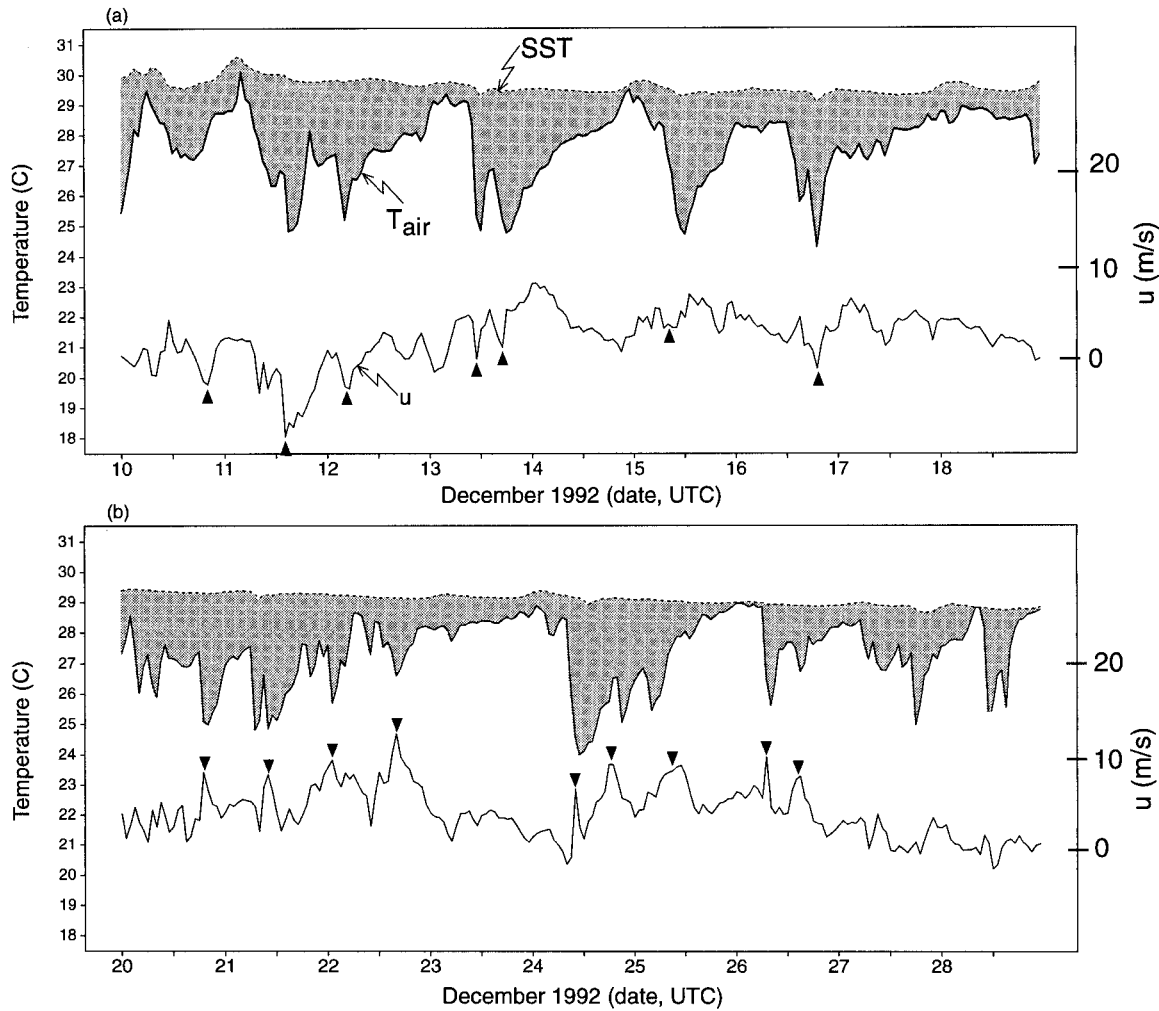


FIG. 5. Data from IMET buoy at  $1.75^{\circ}\text{S}$ ,  $156^{\circ}\text{E}$  during Dec 1992. SST is sea surface temperature,  $T_{\text{air}}$  is the air temperature, and  $u$  is the westerly wind component (negative easterly). Stippling emphasizes times when air was much cooler than ocean surface, i.e., when atmospheric cold pools associated with large rain areas were present. Triangles indicate (a) easterly and (b) westerly wind peaks that seem closely related to cold pools. Data are 10-min averages centered every 10 min. (Adapted from Weller and Anderson 1996.)

scale circulations systematically tended to reduce the surface westerlies. This behavior is consistent with the large-scale shear seen in Fig. 4, which shows easterlies in the mid- to low troposphere in the westerly onset phase of the Kelvin–Rossby wave and a maximum westerly component in the mid- to low troposphere in the strong westerly phase. In subsequent sections of this paper, we will suggest by presentation of ship and aircraft Doppler radar data that the  $u$ -component momentum of the midlevel inflow into large mesoscale convective systems helped to organize the mesoscale circulation of the systems and was transported downward by the organized mesoscale descent below the broad deep stratiform clouds of the mesoscale systems. We organize the discussion by comparing convection in the westerly onset region of the Kelvin–Rossby wave (section 7) with convection in the region of strong westerlies (section 8). The concentrated samples of aircraft and

ship Doppler radar data during these periods (Fig. 3) allowed the two phases of the wave to be compared in some detail.

## 7. Westerly onset region of the Kelvin–Rossby wave: Easterly component midlevel inflows

### a. Basic structure of the easterly component midlevel inflows: The case of 13 December 1992

In the westerly onset phase of the Kelvin–Rossby wave, the midlevel environmental easterlies led to super convective systems over the TOGA COARE region having midlevel inflows from the east (i.e., with an easterly component). Figure 7 shows an example from the N43 aircraft mission of 13 December 1992, which has been

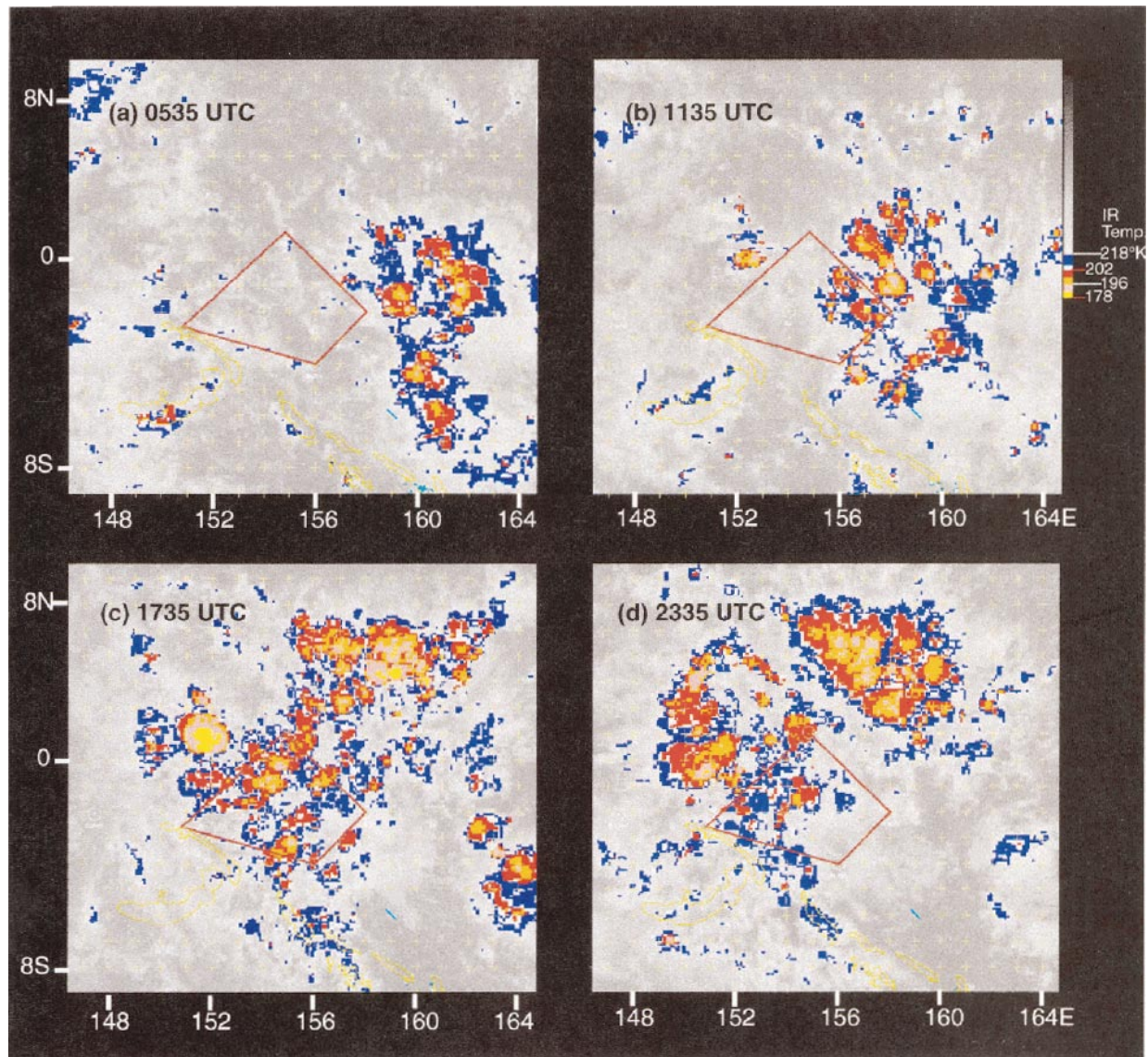


FIG. 6. Infrared imagery from GMS satellite for 11 Dec 1992. Infrared temperature is color coded as indicated by scale in (b). Red trapezoid is the boundary of the TOGA COARE IFA.

analyzed in detail by Chong and Bousquet (1999).<sup>5</sup> The location of this mission with respect to the composite Kelvin–Rossby wave is indicated in Fig. 3. The inset box in Fig. 7a shows the location of the dual-Doppler aircraft radar data with respect to the infrared imagery of the GMS satellite. The cloud shield in the satellite imagery at this time had an area of  $\sim 1.5 \times 10^5 \text{ km}^2$

<sup>5</sup> TOGA COARE ship and aircraft radar data were obtained during the westerly onset period of the Kelvin–Rossby wave on 12–16 December (Fig. 3). We have examined all these cases in detail. The following sections (sections 7a–c) draw on data collected on 13, 14, and 15 December. Data for the cases of 12 and 16 December are consistent with data from 13–15 December but do not add any further information.

covered by a cloud-top temperature of  $< 200 \text{ K}$  and was thus a super convective system by the criterion of Chen et al. (1996). A closer view of the radar reflectivity and dual-Doppler-derived horizontal wind vectors<sup>6</sup> at the 4.4-km level ( $\sim 600 \text{ mb}$ , approximately the melting layer) within the inset region is shown in Fig. 7b. The dual-Doppler-derived horizontal winds within this region of echo at this height were generally easterly, consistent with the ECMWF analyzed ambient large-scale winds at the 500–600-mb levels on this day (Fig. 8) and with the midlevel easterlies in this general region of the

<sup>6</sup> The methods used to produce the dual-Doppler velocity fields used in this study are described in Kingsmill and Houze (1999a).

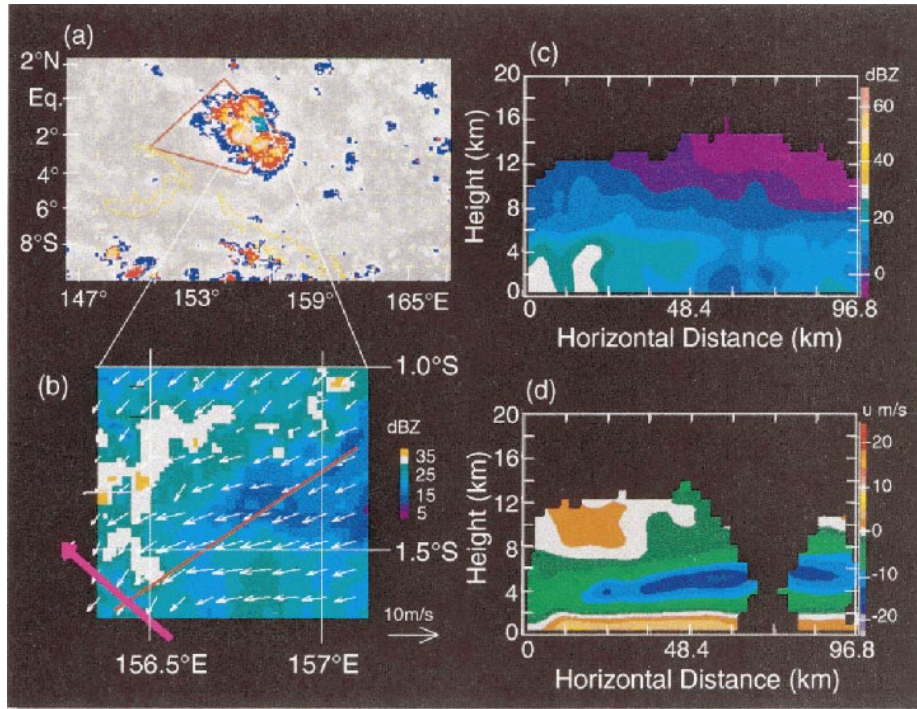


FIG. 7. Dual-Doppler radar data collected by N43 aircraft at about 1700 UTC 13 Dec 1992. (a) The small square inset shows the location of the aircraft data in relation to the color-coded GMS satellite imagery. The polygon outlines the TOGA COARE intensive flux array. (b) Horizontal map of the reflectivity and dual-Doppler winds at the 4.4-km level in the inset of panel (a). Colors indicate reflectivity in dBZ; vectors indicate the horizontal wind. Magenta arrow shows flight track of aircraft during the time the data in the figure were collected. Red line is line of cross sections in (c) and (d). (c) Vertical cross section of reflectivity in dBZ. (d) Cross section of  $u$  component of the dual-Doppler-derived wind. Satellite color scale same as Fig. 9.

Kelvin–Rossby wave composite (Fig. 4a). The winds at the 4.4-km level were confluent within the echo region. The precipitation throughout the region covered by Fig. 7b was primarily stratiform, as can be seen in the vertical cross section of radar reflectivity in Fig. 7c (taken along

the red line in Fig. 7b). A maximum in reflectivity (bright band) was evident at the 4.4-km level, just below the 0°C level. In this cross section, the echo was generally weak, probably in part because of sublimation and evaporation of precipitation particles in the midlevel

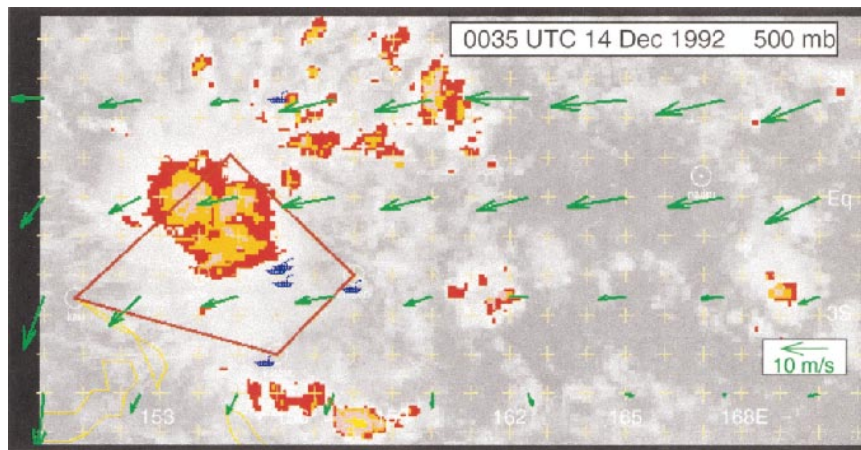


FIG. 8. Infrared satellite image for 0035 UTC 14 Dec 1992. The red–white threshold is at an equivalent blackbody temperature of 208 K. Colors show infrared temperatures at intervals of 6°C. Green arrows show ECMWF winds at 500 mb.

air flowing in from the northeast. The horizontal maps and SW–NE vertical cross sections in Fig. 7 show the same basic flow patterns seen in Figs. 5 and 6 of Chong and Bousquet (1999). They also interpret the weakened echo in the midlevel inflow to be caused by sublimation and evaporation, and they show that the midlevel inflow was part of a mesoscale vortex, which they analyze in some detail.

The midlevel inflow manifested itself strongly in the dual-Doppler-derived west–east ( $u$ ) component of the wind (Fig. 7d). An easterly  $u$ -component jet entered the NE side of the echo region in a layer located between 4 and 6 km. As the jet entered the echo region, it was centered vertically at about 5.5 km ( $\sim 500$  mb, corresponding to Fig. 8). The heights of the upper boundary and core of the  $u$  jet sloped downward as the midlevel inflow extended into the region of echo from NE to SW. This downward-sloping structure of the midlevel inflows penetrating into the stratiform regions of super convective systems entering above the melting layer and sloping down to and below the  $0^{\circ}\text{C}$  level was typical in TOGA COARE (Kingsmill and Houze 1999a). Chong and Bousquet's (1999) dual-Doppler-derived vertical air velocities show that the midlevel inflow was subsiding as it penetrated into the center of the mesoscale system. The magnitude of the easterly  $u$ -component jet in the stratiform region of Fig. 7d was  $\sim 16\text{ m s}^{-1}$ , about 50% stronger than the  $u$  component of the environmental flow indicated in Fig. 8. Also, the  $u$ -component jet in the stratiform region had a closed maximum under the precipitating anvil. It is therefore tempting to infer that as the environmental flow entered the stratiform region it was accelerated inward as it began to subside. However, the accuracy of the synoptic-scale winds is probably insufficient to draw such a conclusion from this comparison alone.

*b. Development of midlevel inflow during the life cycle of a single region of convection: The case of 14 December 1992*

Midlevel inflow into a warm-pool super convective system becomes apparent during the convective-to-stratiform transition of the precipitation pattern. Figures 9 and 10 illustrate this transition in a sequence of events associated with a single region of active convection in a warm-pool super convective system on 14 December 1992.

At the time of Fig. 9, the N42 aircraft was in the center of a developing convective system extending to great heights. The area of Doppler radar observations was near the center of the region where the satellite-observed cloud top was  $<200^{\circ}\text{C}$  (Fig. 9a). Figure 9b shows the radar reflectivity and Doppler-derived horizontal winds at 4.4 km in association with a NW–SE oriented line of intense reflectivity. The vertical cross section of radar reflectivity in Fig. 9c shows that an intense feature within this line was reaching the 18-km

level ( $\sim 80$  mb,  $\sim 192$  K, approximately the tropopause level). The corresponding cross section of  $u$ -component velocity in Fig. 9d shows a layer of westerly inflow, extending from the surface to  $\sim 4$  km, rising over a downward-sloping easterly component flow in the apparent cold pool. Inflows to the updrafts of deep convection in TOGA COARE averaged  $\sim 3$  km in thickness and were never less than about 1 km (Mapes and Houze 1995; Kingsmill and Houze 1999a); that is, the inflow layer was typically much deeper than the planetary boundary layer. The dual-Doppler computation of the divergence and vertical velocity fields confirm that the upward-sloping westerly current was an updraft, and the downward-sloping easterly current was a downdraft (Fig. 9e).

Two hours after the time of Fig. 9, N42 was flying in the same geographical region, after the convective region seen earlier was in a highly evolved state. Data from this second pass are in Fig. 10. Figure 10a shows that the area covered by infrared-estimated cloud-top temperature  $<200^{\circ}\text{C}$  was somewhat less than at the earlier time. Radar echo top (i.e., the top of the precipitation layer) was generally about 14 km (Fig. 10c), compared with 18 km at the earlier time. The echo had become highly stratiform, with a pronounced and intense bright band at the melting layer. An easterly midlevel inflow extended across the  $u$ -component velocity cross section in Fig. 10d. It had a closed maximum of horizontal velocity and generally resembled the  $u$ -component jet in the stratiform region of the mesoscale convective system observed the previous day (cf. Fig. 7d). The melting layer and easterly component jet were accompanied by a distinct layer of convergence at about the melting level, as was typical of stratiform regions of mesoscale convective systems in TOGA COARE (Mapes and Houze 1995).

The aircraft data in Figs. 9 and 10 are unique in the way that they capture two stages in the evolution of the precipitation and wind in a super convective system dominated by a single region of deep convection. From the change in reflectivity and velocity between Figs. 8 and 9, it appears that one region of convection produced one region of midlevel inflow. In this relatively small (in terms of horizontal area) super convective system, one region of convection dominated and the midlevel inflow did not cover a huge region. The 15 December cloud system, observed about 24 h after that shown in Figs. 9 and 10, provides an opportunity to see how a group of convective elements like the one depicted in Figs. 9 and 10 collectively developed into a broader system with the stratiform region and midlevel inflow jet covering a much larger region.

*c. Development of mesoscale midlevel inflow from a group of convective elements: The case of 15 December*

1) OVERVIEW

The life history overview of the 15 December cloud system, as seen in infrared satellite imagery (Fig. 11),

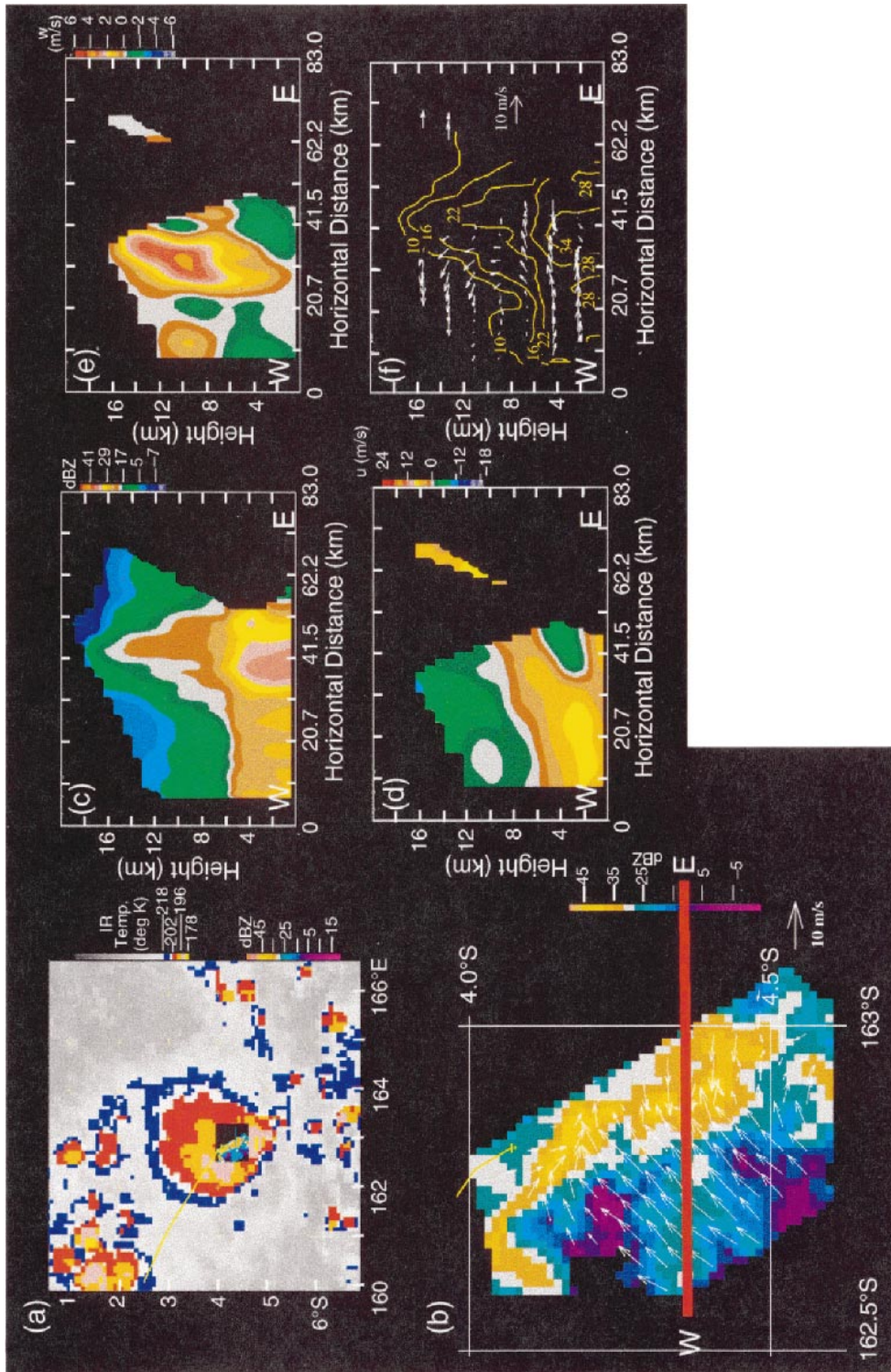


FIG. 9. Dual-Doppler radar data collected by N42 aircraft at about 1630 UTC 14 Dec 1992. (a) The small square inset shows the location of the aircraft radar data obtained at the 4.4-km level at about 1630 UTC in relation to the color-coded GMS satellite imagery. A 40-min segment of the flight track prior to 1630 is shown by the yellow line. The polygon outlines the TOGA COARE intensive flux array. (b) Horizontal map of the reflectivity and dual-Doppler winds at the 4.4-km level in the inset square of panel (a). Colors indicate reflectivity in dBZ; vectors indicate the horizontal wind. Red line (W-E) is line of cross sections in (c)–(e). (c) Vertical cross section of reflectivity in dBZ. (d) Cross section of  $u$  component of the dual-Doppler-derived wind. (e) Cross section of vertical component ( $w$ ) of the dual-Doppler-derived wind. (f) Vertical cross section showing vector wind in W-E cross section overlaid on reflectivity (dBZ) contours.

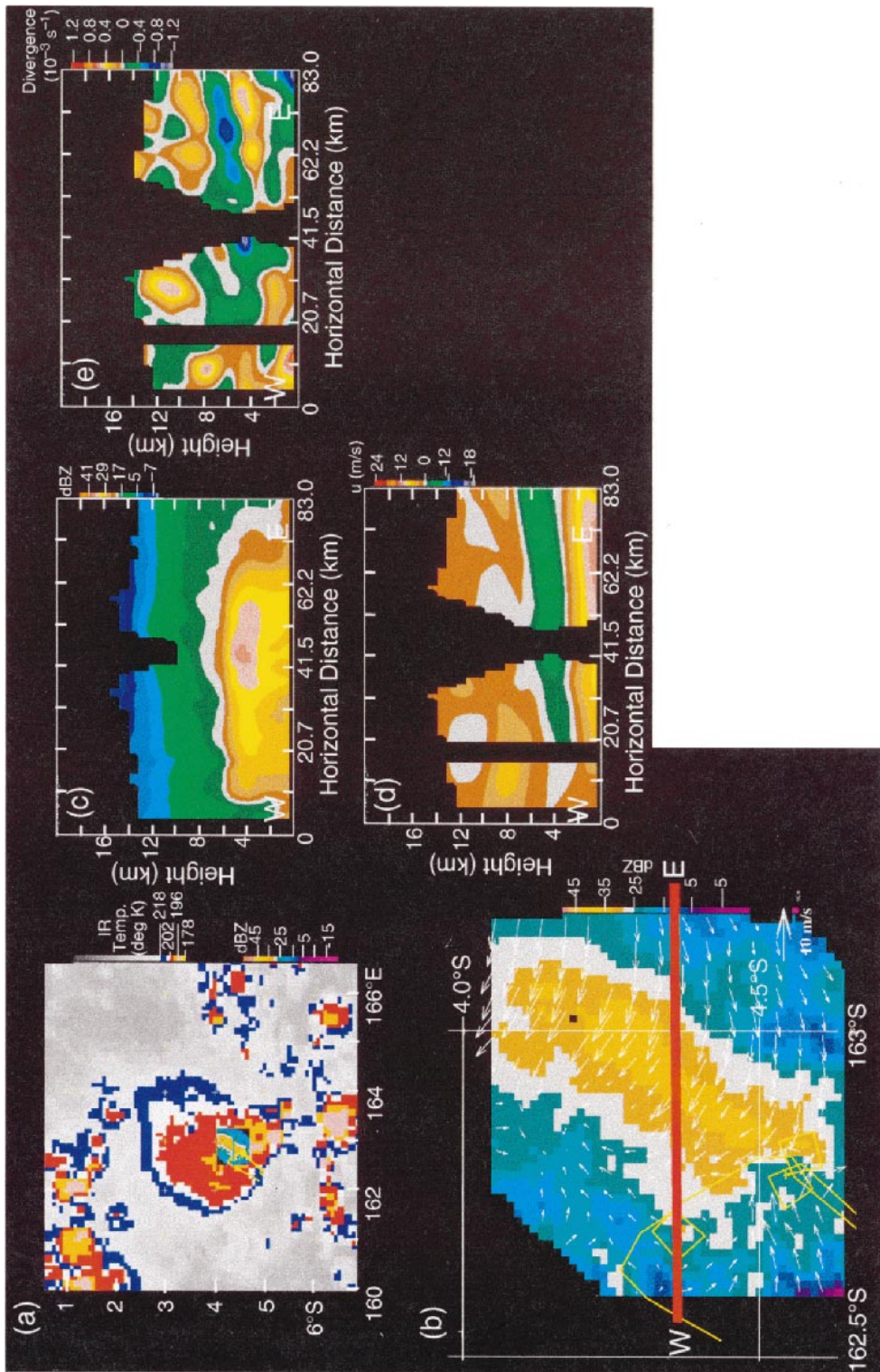


FIG. 10. Dual-Doppler radar data collected by N42 aircraft at about 1830 UTC 14 Dec 1992. (a) The small square inset shows the location of the aircraft radar data obtained at about 1830 UTC in relation to the color-coded GMS satellite imagery. A 40-min segment of the flight track prior to 1830 UTC is shown by the yellow line. The polygon outlines the TOGA COARE intensive flux array. (b) Horizontal map of the reflectivity and dual-Doppler winds at the 4.4-km level in the inset square of (a). Colors indicate reflectivity in dBZ; vectors indicate the horizontal wind. Red line (W-E) is the line of cross sections in (c)-(e). (c) Vertical cross section of reflectivity in dBZ. (d) Cross section of the dual-Doppler-derived wind. (e) Cross section of horizontal divergence (cold colors show convergence) of the dual-Doppler-derived wind.

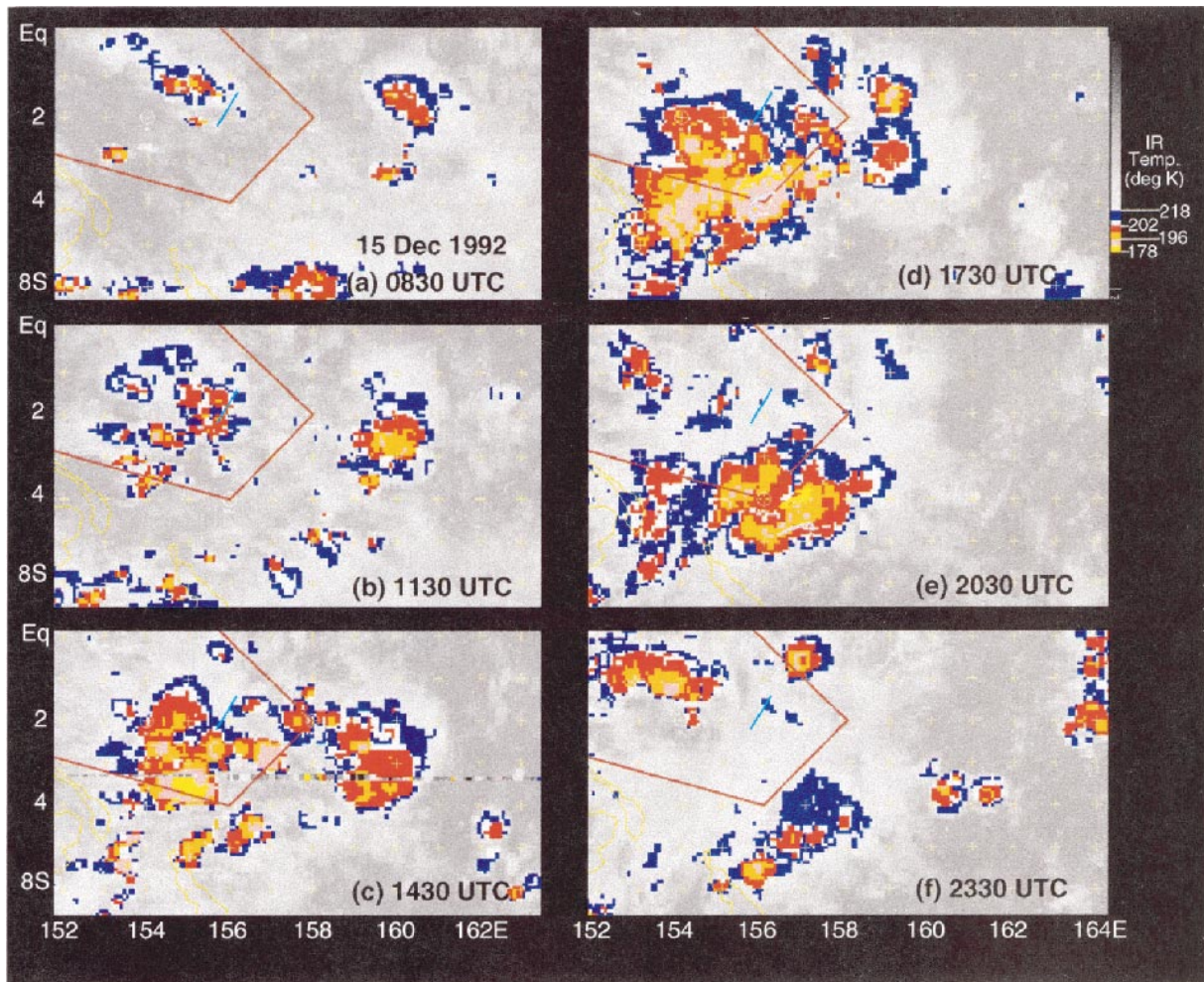


FIG. 11. Sequence of infrared satellite imagery for 15 Dec 1992.

suggests that the system began as a group of discrete convective-scale elements reaching great heights (the red indicates cloud-top temperature  $<202$  K). These elements begin forming at about 0600–0700 UTC, and through 1130 UTC remained discrete (Figs. 11a,b). Thus, the region of the warm pool within the IFA boiled with these deep convective elements for about 6 h prior to 1200 UTC (about midnight over the IFA), at which time the cloud system began to take on a more unified appearance. By 1430 UTC (Fig. 11c), the extremely cold cloud top had become a contiguous mesoscale region of cloud-top temperature  $<202$  K, with portions  $<190$  K. This contiguous cold-cloud-top region reached maximum size at about 1730 UTC (Fig. 11d). The ship *Xiangyanghong #5* was located in the center of the developing region, and the ship radar observed the structure of the precipitation and Doppler radial velocity throughout the multihour developmental stage of this system. The N42 and N43 Doppler radar aircraft arrived at about 1630 UTC. The satellite data 1 h later (Fig. 11d) show that the mesoscale cloud system was fully

developed at about this time. The size of the cold cloud top in Fig. 11d would qualify as a super convective system in the terminology of Chen et al. (1996). However, during most of the time the aircraft were flying, the cloud system was weakening. The aircraft flew in the southern portion of the cloud system until about 2100 UTC. During this time, the satellite-observed cloud top was generally warming and shrinking (Figs. 11d–f).

Figures 12 and 13 show hourly horizontal maps of radar reflectivity and radial velocity from the *Xiangyanghong #5* for the 0.5-km level during the period 1035–1835 UTC, when the satellite-observed cloud system (Fig. 11) was converting itself from a group of discrete convective cells to a more contiguous mesoscale convective system. Up to 1135 UTC, the precipitation pattern was dominated by intense convective reflectivity cores (Figs. 12a,b). Although the echo at 1135 UTC was nearly contiguous over the radar area, it retained an almost completely convective character consisting of

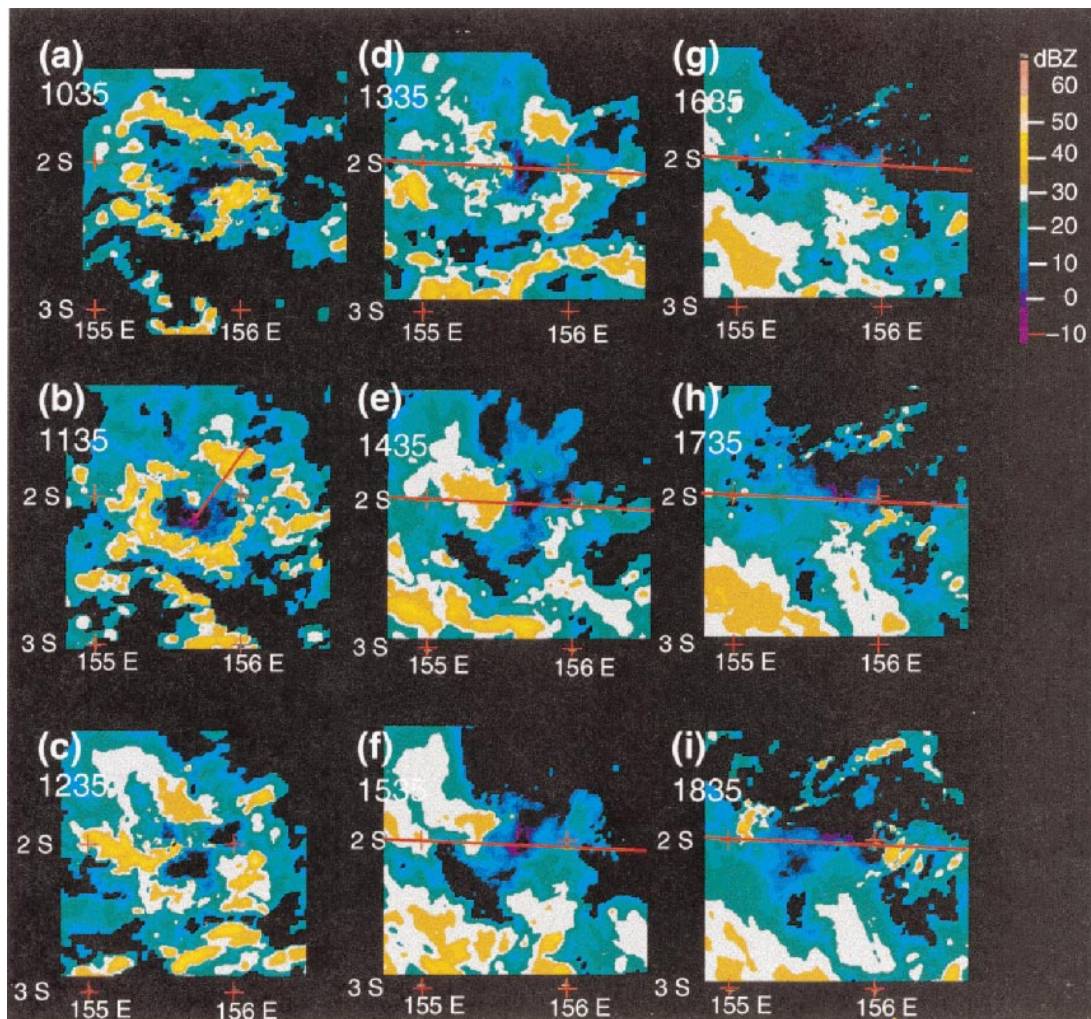


FIG. 12. Sequence of radar reflectivity data (dBZ) at the 0.5-km level obtained on 15 Dec 1992 with the radar on the ship *Xiangyanghong #5*. Red lines locate cross sections shown in Fig. 19.

intense echo cores interconnected by relatively weak echo.

## 2) CONVECTIVE CORES IN THE EARLY STAGES OF THE MESOSCALE CONVECTIVE SYSTEM

At 1135 UTC, the low-level westerly wind was surging to  $\sim 14 \text{ m s}^{-1}$  over the whole rain area (Fig. 13b). Convection had been active for  $\sim 5\text{--}6$  h in the region. In this section we examine the reflectivity and internal air motions to determine whether they behaved systematically in such a way as to affect the larger-scale wave dynamics.

Figure 14 shows the ship radar data in a SW–NE cross section through one of the convective elements to the northeast of the ship. The reflectivity cross section (Fig. 14a) shows a very deep echo core. The velocity cross section (Fig. 14b) exhibits a structure typical of deep convective echo cores observed throughout TOGA

COARE (Kingsmill and Houze 1999a). A strong divergence signature appears at cell top;<sup>7</sup> an increase in radial velocity with increasing range of about  $10 \text{ m s}^{-1}$  over a distance of  $\sim 15 \text{ km}$  suggests a divergence of  $\sim 10^3 \text{ s}^{-1}$ . At low levels, a strong convergence signature appears at the northeastern edge of the cell; a decrease in radial velocity with increasing range of about  $10 \text{ m s}^{-1}$  over a distance of  $\sim 5 \text{ km}$  suggests a gust front convergence of  $\sim 2 \times 10^3 \text{ s}^{-1}$ . Just forward of the center of the rain shaft and behind the gust front, the westerly component velocity was maximum, consistent with a hydrostatic pressure maximum in the rain shaft producing a forward acceleration, locally enhancing the low-level westerly

<sup>7</sup> Extensive examination of dual-Doppler wind fields from the TOGA COARE aircraft radars confirms that the upper divergence pattern at the tops of convective cells was typically a quasi-axisymmetric pure divergence field.

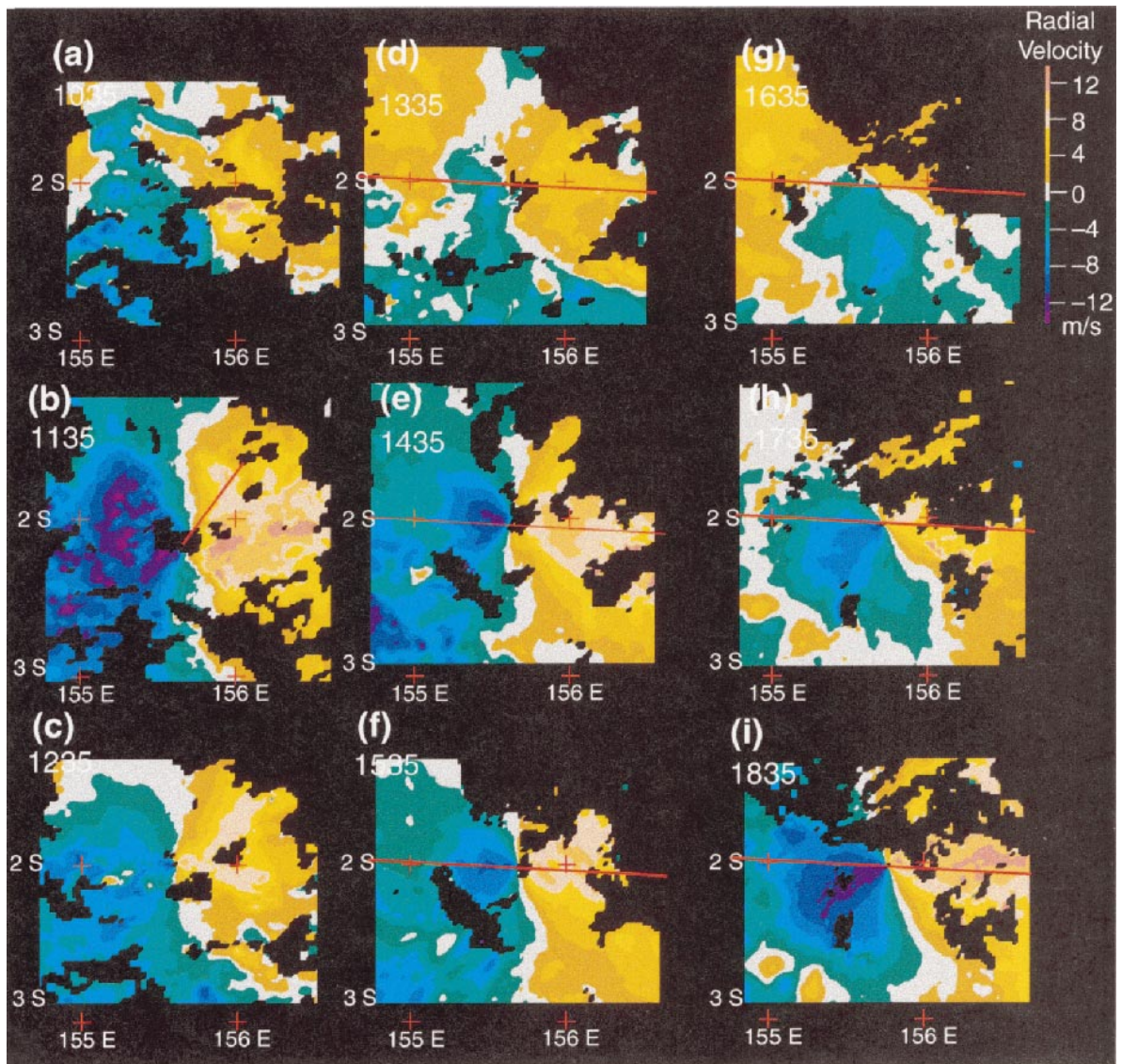


FIG. 13. Sequence of Doppler radar radial velocity ( $\text{m s}^{-1}$ ) at the 0.5-km level obtained on 15 Dec 1992 with the radar on the ship *Xiangyanghong* #5. The radar is at the center of the plot. Cold colors indicate radial velocity toward the ship radar. Warm colors indicate radial velocity away from the radar. Gray indicates zero radial velocity. The color pattern indicates a generally westerly wind across the ship at all times. Red lines locate cross sections shown in Fig. 19.

flow and bolstering the gust front. Lying just above the low-level westerly component current was a layer of easterly component air, evidently rising in the updraft into the region of divergence at the top of the convective echo. Apparently, the convective element systematically transported easterly component momentum upward in the updraft. This structure was seen in the convective echoes observed by the ship radar during the early hours of the mesoscale system (starting about 0600 UTC).

### 3) CONVECTIVE CORES IN THE MATURE AND LATE STAGES OF THE MESOSCALE CONVECTIVE SYSTEM

Deep convective echoes of this type continued to form after 1135 UTC, during the time in which the satellite-

observed cloud system was converting itself from a group of discrete convective clouds to a more contiguous mesoscale convective system ( $\sim 1130$ – $1430$  UTC; Figs. 11b,c) and on through its dissipating stages (Figs. 11d–f). The N42 research aircraft arrived in the southern part of the mesoscale convective system at about 1630 UTC, when the super convective system was reaching maturity (Fig. 11d). It was at this time that the deepest convective element documented by research radar in TOGA COARE was observed by the aircraft radar. The dual-Doppler data for this convective echo are shown in Fig. 15. Echo top was over 18 km, and the 30-dBZ echo was reaching 14 km (Fig. 15a). The echo core sloped generally toward the west with increasing height.

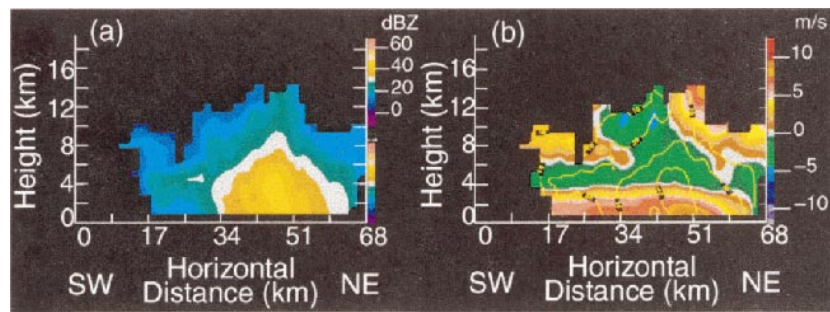


FIG. 14. Vertical cross sections for data obtained at about 1135 UTC 15 Dec 1992 by the radar on the *Xiangyanghong #5*. Cross section runs SW–NE along the line shown in Fig. 13b. (a) Radar reflectivity (dBZ). (b) Doppler radial velocity. Faint yellow contours in (b) repeat the radar reflectivity contours shown in (a).

Dual-Doppler synthesis showed a sloping layer of convergence matching the slope of the echo (Fig. 15b). It also showed strong divergence at cell top and in the apparent cold pool below the convergence layer. This divergence pattern implied an updraft of over  $10 \text{ m s}^{-1}$  in the upper portion of the echo, with maximum intensity at the 10–15-km levels (Fig. 15c). The  $u$  component of the wind was easterly in the sloping updraft and strong westerly in the cold pool, with a local maximum of westerly component in the cold pool just behind the gust front (Fig. 15d). This  $u$ -component field was quite similar to the radial velocity pattern seen by the ship radar 5 h earlier (Fig. 14b). Figure 16 shows aircraft dual-Doppler data for a cell observed on the southern side of the system at about the time of Fig. 11e. These cross sections show the same momentum transport behavior seen at the earlier times: The updraft seen in Fig. 16b contained air with an easterly  $u$ -component of momentum (Fig. 16c), and an enhanced westerly component again occurred at low levels behind the near-surface gust front. The momentum transport associated with convective-scale cores was typically observed in the sense seen in these examples, although on at least one occasion a convective element developed with an opposite slope and correspondingly opposite sign of vertical convective-scale momentum transport compared to neighboring convective cells (Kingsmill and Houze 1999a). Thus, the convective-scale momentum transports were not entirely systematic even in the same part of a mesoscale convective system.

#### 4) LATERAL SPREADING OF ICE BY CONVECTIVE ELEMENTS

The divergence evident near the top of the convective echo in Figs. 14b and 15b was a common signature of all the convective echoes observed by Doppler radar from the formative through the mature stage of this mesoscale convective system. Also, the reflectivity was quite high at the levels where the divergence was occurring. In Fig. 14a, echo top was 14 km, and the 30-dBZ echo contour extended above the 8-km level. In

Fig. 15a, echo top was over 18 km, and the 30-dBZ echo reached 14 km. Together with the strong vertical velocities present at high levels and the fact that the  $0^\circ\text{C}$  level is at the 5-km level over the warm pool, these observations indicate a large content of frozen precipitation (probably graupel) at mid- to upper levels. The strong vertical air motions were transporting this ice upward, and the divergence at upper levels was spreading it laterally through a deep layer about 8 km deep lying between  $\sim 10$  and 18 km (not a thin cirrus veil).

A further illustration of the robust ice divergence in this super convective system is shown by the radar data on the *Xiangyanghong #5* at 1235 UTC along the WNW–ESE line in Fig. 17, which is a horizontal map of the Doppler radial velocity at the 13.5-km level. Figure 18 contains vertical cross sections of reflectivity and radial velocity along this line. Figure 18b shows the radial-velocity divergence near the tops of two active convective echoes. These two echoes had a velocity difference of  $\sim 10 \text{ m s}^{-1}$  over 10–30 km. This divergence existed through a layer typically 5 km deep. Taking  $100 \text{ km}^2$  as a typical area covered by the divergence signature and supposing that the ice mass content of the air in the divergent layer in the upper portion of a cell was  $1 \text{ g m}^{-3}$ , we obtain a net ice mass divergence of  $\sim 2 \times 10^{13} \text{ g}$  in 5 h. If five of these convective elements were present over a  $100 \text{ km} \times 100 \text{ km}$  area at any given time in a 5-h period, which was about the duration of the convective early stage of the 15 December cloud system ( $\sim 0700$ – $1200$  UTC), then enough ice would have diverged from the upper portions of convective elements to fill the  $5 \text{ km} \times 100 \text{ km} \times 100 \text{ km}$  region with an average ice mass content of  $0.4 \text{ g m}^{-3}$ . Thus, the developmental period of the 15 December cloud system leading up to 1230 UTC (Figs. 11b,c, 12c, and 13c) was about the time required for the persistent deep convective cells [acting as “particle fountains” in the terminology of Yuter and Houze (1995)] to fill a large region of the mid- to upper troposphere with a dense ice cloud, and it was at about this time that the satellite data showed the upper-level extremely cold cloud tops merging into a continuous mesoscale sheet.

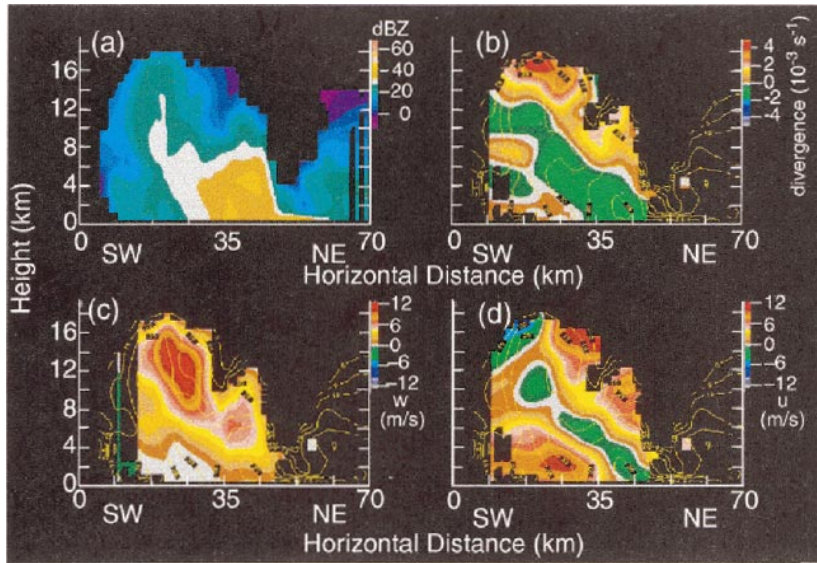


FIG. 15. Vertical cross sections for data obtained at about 1647 UTC 15 Dec 1992 by the dual-Doppler radar system on the N42 aircraft. Cross section runs SW–NE through an extremely deep convective cell. (a) Radar reflectivity (dBZ). (b) Horizontal divergence ( $s^{-1}$ ). (c) Vertical component ( $w$ ) of the dual-Doppler-derived wind. (d) Zonal component ( $u$ ) of the dual-Doppler-derived wind. Faint yellow contours in (b)–(d) repeat the radar reflectivity contours shown in (a).

5) GROWTH OF ICE PARTICLES IN THE DEVELOPING MESOSCALE CIRCULATION

Buoyant parcels expand as they rise. Parcels that were on the order of a kilometer in horizontal dimension at the top of the boundary layer increase in width by orders of magnitude by the time they arrive at upper levels. (Updraft cells are not columns but rather inverted cones, tilting as required by ambient shear.) The divergence of ice mass, just discussed, is a manifestation of this expansion of the rising parcels. Another manifestation of the expansion is that the upper troposphere of the region containing convective elements becomes filled with slightly buoyant saturated air. Thus a mesoscale region of the upper troposphere becomes positively buoyant, and mesoscale circulations can develop. The ice particles suspended in and slowly falling through this grad-

ually ascending air can grow into larger precipitation particles and become an incipient stratiform precipitation region.

This process accounts for the events occurring after about 1230 UTC on 15 December 1992 (Figs. 12c, 13c). The precipitation filling the regions between active convective cells had begun to change character significantly, with a rather sudden appearance over a larger area of enhanced, moderate-intensity stratiform radar echo between active cells. Tracking of echoes in time lapse indicates that these areas did not appear as the simple collapse of convective cells. Apparently, the upper-level cloud deck, which had become a broad continuous sheet at about 1430 UTC (Fig. 11c), had become able to support the growth of ice particles formed in and diverged out from the intense convective cells populating the cloud system.

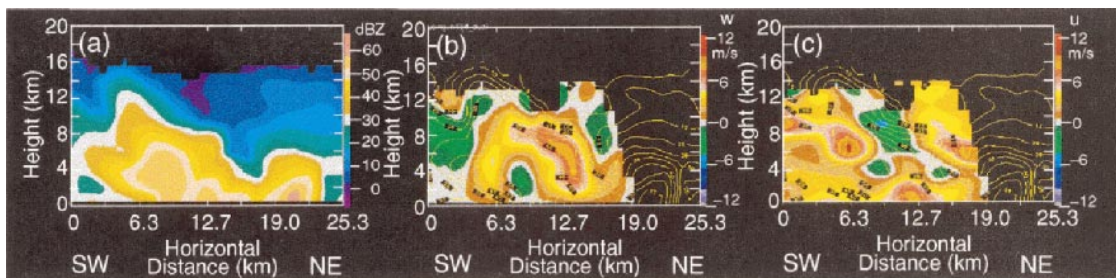


FIG. 16. Vertical cross sections for data obtained at about 2002 UTC 15 Dec 1992 by the dual-Doppler radar system on the N43 aircraft. Cross section runs SW–NE through an extremely deep convective cell. (a) Radar reflectivity (dBZ). (b) Vertical component ( $w$ ) of the dual-Doppler-derived wind. (c) Zonal component ( $u$ ) of the dual-Doppler-derived wind. Faint yellow contours in (b) and (c) repeat the radar reflectivity contours shown in (a). They are shown for reference only.

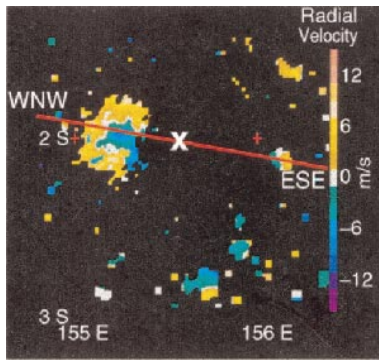


FIG. 17. Doppler radial velocity ( $\text{m s}^{-1}$ ) at the 13.5-km level obtained at 1235 UTC 15 Dec 1992 with the radar on the *Xiangyanghong* #5. Ship location is marked by **x**. Red lines locate cross sections in Fig. 18.

#### 6) ENHANCEMENT OF THE MIDLEVEL INFLOW BY ICE PARTICLES FALLING OUT OF THE THICK UPPER CLOUD DECK

At about the same time that the upper troposphere filled with positively buoyant air, the lower troposphere evidently became largely negatively buoyant. Remnants of convective downdrafts accumulating in lower levels spread out, and the evaporation, melting, and sublimation of precipitation particles falling out of the stratiform ice-cloud deck aloft further cooled the air at lower levels. Thus, the natural result of an ensemble of deep tropical convection is to form a two-layer (buoyant aloft, negatively buoyant at lower levels) stratiform region (Mapes and Houze 1995; Houze 1997).

The structure of the stratiform region may have been enhanced by a positive feedback of mesoscale microphysics and large-scale shear. Kingsmill and Houze (1999a) found that midlevel inflow entered the cloud system from the direction that the relative flow toward the anvil was greatest and was best defined in a layer immediately under the sloping base of the anvil, suggesting that cooling by sublimation of ice particles falling from the upper-level cloud was a key factor in form-

ing and enhancing the inflow [as suggested by the model calculations of Braun and Houze (1997)]. Ambient air enters the system at upper levels, above the  $0^{\circ}\text{C}$  level, and descends along the bottom edge of the anvil to the melting level, where it undergoes further cooling and enhancement by the melting cooling [model calculations of Yang and Houze (1995)].

#### 7) MOMENTUM TRANSPORT BY THE MIDLEVEL INFLOW

The subsiding midlevel inflow, organized by large-scale environmental shear and intensified by latent cooling in the stratiform precipitation region of the super convective system, transports midlevel environmental easterly momentum downward. Figure 19 shows a series of cross sections taken at 1-h intervals along the approximately west–east line shown in Figs. 13d–i. The ship position is near the center of the cross section line. Warm colors indicate radial velocities away from the ship and cold colors velocities toward the ship. In Fig. 19a, the radial velocities at midlevels approach from the east; then downwind of the ship they slope down to near the sea surface. This structure is consistent with Fig. 13d, which shows that the low-level radial velocities were generally easterly to the west of the ship and westerly to the east of the ship (warm colors both east and west of the ship). For the next two hours (1435 and 1535 UTC) the low-level flow was westerly both east and west of the ship (Figs. 13e,f). Figures 19b,c show that the midlevel easterly jet at these times was elevated, extending only a short distance beyond the ship and not penetrating to the surface. At 1635 UTC the easterly jet again sloped down to the surface and the patterns in Figs. 13g and 19j were nearly a repeat of those seen 3 h earlier. From 1735 to 1835 UTC, the layer of easterly flow again rose up to midlevels (Figs. 19e,f) and the low-level winds west of the ship again became westerly (Figs. 13h,i).

The momentum transport evident in Figs. 13 and 19 is reasonable in terms of what is generally known about

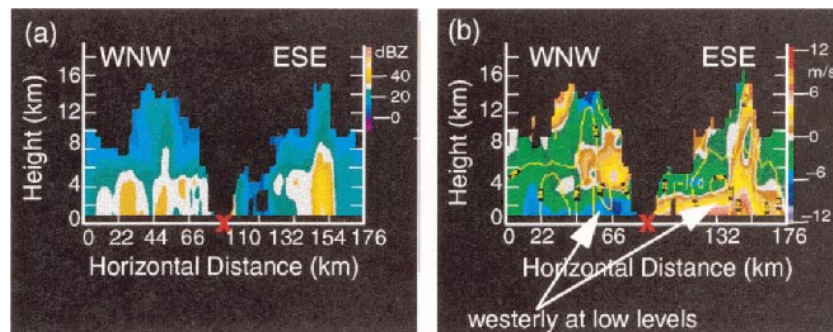


FIG. 18. Vertical cross sections of data obtained at 1235 UTC 15 Dec 1992 with the radar on the *Xiangyanghong* #5. Sections are along the WNW–ESE line in Fig. 17. (a) Radar reflectivity (dBZ). (b) Doppler radial velocity ( $\text{m s}^{-1}$ ). Yellow contours repeat the reflectivity pattern. Ship location is marked by red **x**.

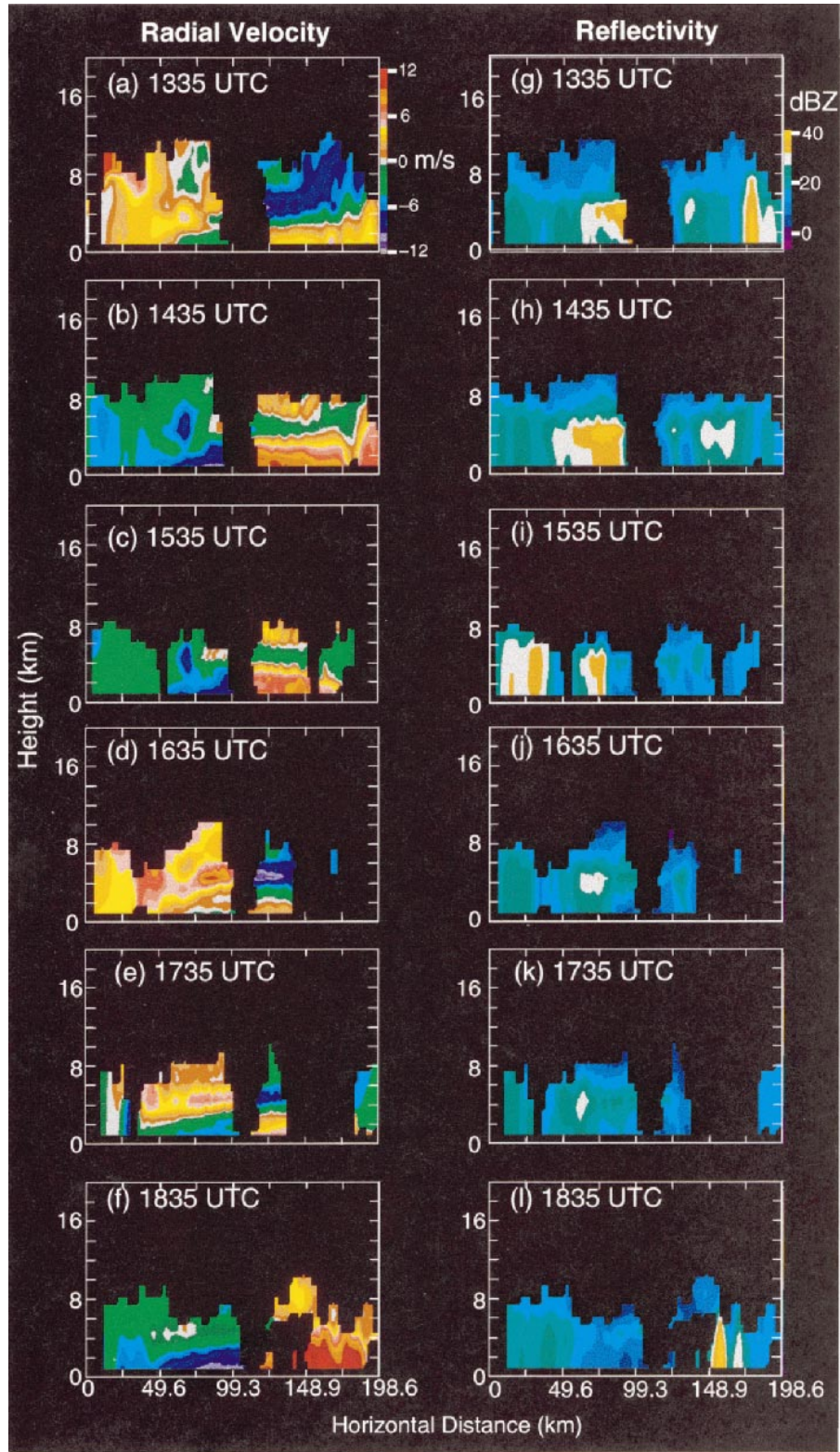


FIG. 19. Cross sections of radial velocity and reflectivity from the radar on the ship *Xiangyanghong #5* on 15 Dec 1992. Cross sections are along the lines shown in Figs. 12 and 13.

the stratiform regions of mesoscale convective systems (e.g., Houze 1989). Apparently, the mesoscale midlevel inflow air, which most of the time lay some short distance above the 0.5-km level, was temporarily advected downward (over periods  $\sim 1$  h) at 1335 and again at 1635 UTC. A vertical velocity of  $\sim 30$  cm s accounts for a downward advection of  $\sim 1$  km over a 1-h period. A downward vertical velocity of this magnitude would not be surprising in a robust stratiform region. Furthermore, mesoscale horizontal pressure gradients (LeMone 1983; Smull and Houze 1987) could further accelerate the easterly component of the subsiding midlevel inflow during an hour's time.

This behavior of the midlevel inflow, as it subsides and brings easterly momentum downward to very low levels, is a negative feedback to the large-scale flow. When these mesoscale easterly flows come down to low levels, they contribute an easterly component to the large-scale average wind at low levels. This behavior explains the IMET buoy data shown in Fig. 5. This easterly transport to low levels runs counter to the tendency of westerlies to become established in this westerly onset region of the Kelvin–Rossby wave. We further note that the vertical transport of momentum by the easterly midlevel inflow was opposite to the convective-scale momentum transports occurring in the individual convective cells (Figs. 14–16), in which the updrafts systematically carried easterly momentum upward at all stages of the mesoscale convective system. It is as if the highly organized mesoscale midlevel inflow of the super convective system were acting as a brake on the development of low-level westerlies in this phase of the Kelvin–Rossby wave.

## 8. Strong westerly region of the Kelvin–Rossby wave

### a. Basic structure of the westerly component midlevel inflow

The behavior of the super convective systems in the strong westerly phase of the Kelvin–Rossby wave was observed by the ship Doppler radars during 20–27 December 1992 and 11 February 1993 (Fig. 3). The December period corresponds to the westerly wind burst and maximum of convective activity accompanying the passage of the first Kelvin–Rossby wave system of TOGA COARE (Fig. 2a). It also corresponds to the time period examined by Moncrieff and Klinker (1997) in their modeling study. The February period was associated with the westerly wind burst of the second Kelvin–Rossby wave system of TOGA COARE (Fig. 2b). The super convective systems in this regime had westerly component midlevel inflows. This different behavior is consistent with the large-scale ambient flow; Fig. 4 shows that the large-scale  $u$ -component wind profile in this part of the late-December Kelvin–Rossby wave was westerly through a deep layer, up to the 9–

10-km ( $\sim 300$  mb) level, with a maximum at the 1–3-km ( $\sim 900$ –750 mb) level. Figure 3 of Lin and Johnson (1996) and Fig. 4 of Chen et al. (1996) show a similar deep layer of westerlies in February 1993.

An example of the mesoscale midlevel inflow that developed in the precipitation regions of super convective systems in this environment is found within the 24 December 1992 case, shown in Fig. 20 as observed by the radar aboard the ship *Vickers*. The flow at 0.5-km level was from the southwest at  $\sim 15$ – $20$  m s $^{-1}$  (inset of Fig. 20a). Figure 20b indicates that a contiguous rain area covered most of the 200 km  $\times$  200 km area of the inset box in Fig. 20a.

Figure 20c is a vertical cross section through the reflectivity field along the NW–SE line segment in Fig. 20b. The northwest half of the cross section shows stratiform precipitation, indicated by the bright band at the 4.5-km melting level. The stratiform precipitation was interrupted by convection, with a strong reflectivity core 55–70 km from the radar. The reflectivity was strongest below 6–7 km, but the echo extended up to 16 km.

Figure 3 suggests that the data collected by the ship radar on 24 December were obtained in the part of the Kelvin–Rossby wave where the low to midlevel flow was from the northwest (in the southwest quadrant of the northern gyre in the streamline pattern). The radial velocity cross section (Fig. 20d) correspondingly showed a well-defined NW-to-SE midlevel inflow entering the NW side of the precipitation area at the 6-km level, above the melting layer. The NW-to-SE orientation of the cross section was chosen for illustration because the radial wind magnitude at midlevels was maximum along this section, indicating that the cross section parallels the midlevel inflow. The axis of maximum northwesterly midlevel inflow steadily dropped toward the SE, crossing the melting layer, and reaching near the surface in the region of the deep convective cell on the SE end of the cross section. The radial velocity in the upper portion of the intense convective cell exhibits a single-Doppler divergence signature with a strong horizontal gradient of radial velocity between 8 and 16 km. Above 12 km, the radial flow is toward the radar on the NW side of the cell and away from the radar on the SE side of the cell. At low levels, the magnitude of the northwesterly radial velocity in the region of the convective cell is enhanced, which we suggest is the direct result of downward transport of momentum, probably aided by the downward-sloping midlevel inflow jet. This process is similar to that seen on 15 December (Figs. 13 and 19), except in the sign of the momentum transport. On 24 December the downward-sloping mesoscale midlevel inflow transported northwesterly momentum downward, enhancing the already strong westerlies found at lower levels in this region of the Kelvin–Rossby wave. This downward transport was probably more than simple downward advection of the environmental midlevel northwesterly

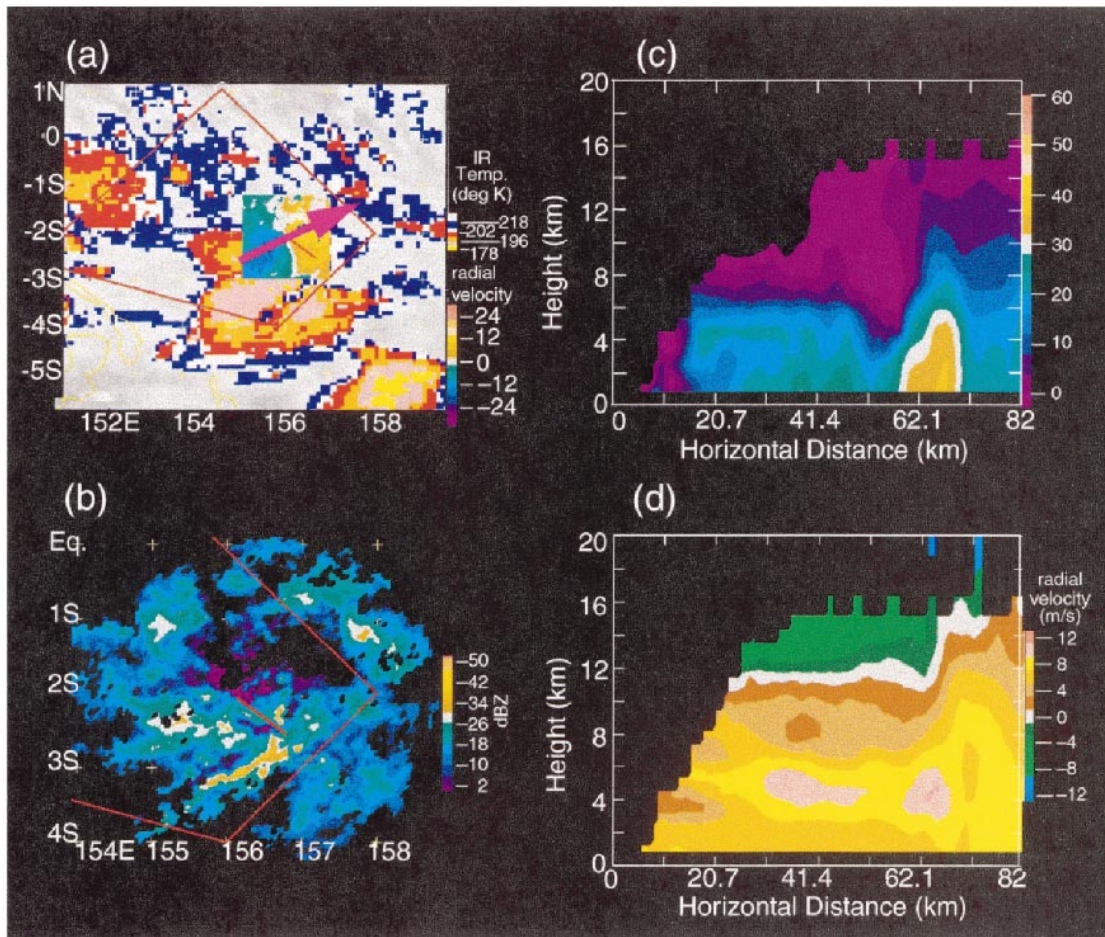


FIG. 20. Radar data obtained at about 1800 24 Dec 1992 from the *Vickers*. (a)  $0.8^\circ$  elevation scan of radial velocity superimposed on color-coded GMS satellite infrared temperature (same color scale as in Fig. 9). The inset square contains data from the *Vickers* radar, for which the cool shades indicate radial velocity toward the radar (located in the center of the square), and warm shades indicate radial velocity away from the radar. The arrow indicates the southwesterly direction of the low-level wind at the ship that is consistent with the radial velocity field. (b)  $0.8^\circ$  elevation angle scan of reflectivity for the region of radar data in (a). A NW-SE azimuth line starting at the radar is shown. The ship is at the NW end of the line. (c) Vertical cross section of radar reflectivity (dBZ) along the NW-SE azimuth in (b). (d) Vertical cross section of radial velocity along the NW-SE azimuth in (b).

wind. The environmental northwesterlies probably accelerated when they entered the system as a result of mesoscale low pressure perturbations internal to the cloud system.

The super convective system observed on 11 February 1993 in TOGA COARE (Fig. 3) provides an independent check on the conclusions drawn from the 24 December 1993 system. The large amount of precipitation from this system and the structure of the precipitation pattern observed by the TOGA COARE ship radars have been described by Halverson et al. (1999). They did not analyze the Doppler radial velocity data that document the midlevel inflow of this important storm. Figure 21 presents the Doppler radial velocity data along with horizontal and vertical cross sections of radar reflectivity and infrared satellite data. The data are presented in the same format as Fig. 20. The radial

velocity structures in Fig. 21 are strikingly similar to those in Fig. 20, indicating that the midlevel inflows were organized and transporting momentum in a manner nearly identical to the super convective systems in the December Kelvin-Rossby wave.

These cases of ship-based Doppler radar in two separate Kelvin-Rossby wave events in TOGA COARE indicate that the organized mesoscale midlevel inflows to super convective systems in the westerly wind core between the two large-scale Rossby gyres systematically increase the already strong low-level westerlies. This result based only on observations is entirely consistent with Moncrieff and Klinker's (1997) model results suggesting that the organized downdrafts of super clusters enter from a direction determined by the large-scale dynamics and act to increase the low-level westerlies in this part of the wave structure.

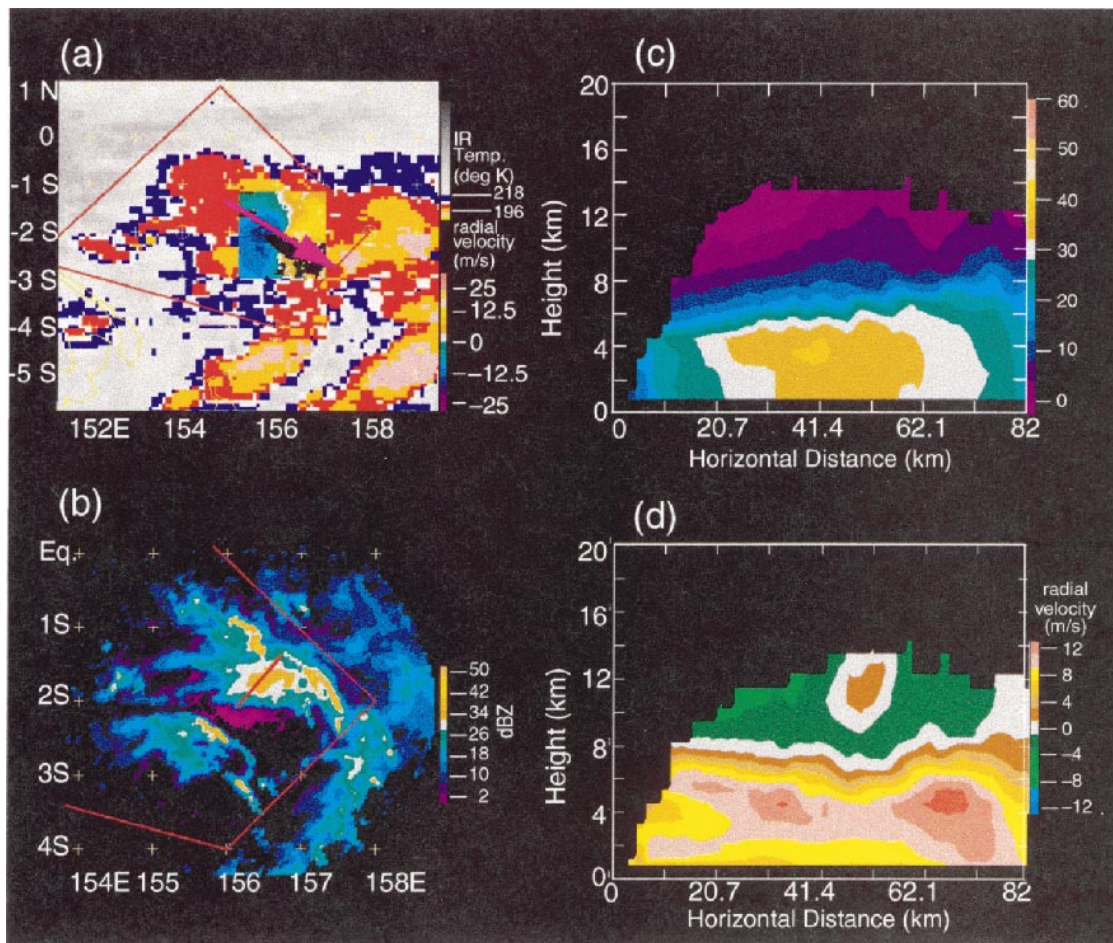


FIG. 21. Radar data obtained at about 1542 UTC 11 Feb 1993 from the *Vickers*. (a)  $0.8^\circ$  elevation scan of radial velocity superimposed on color-coded GMS satellite infrared temperature (same color scale as in Fig. 9). The inset square contains data from the *Vickers* radar, for which the cool shades indicate radial velocity toward the radar (located in the center of the square), and warm shades indicate radial velocity away from the radar. The arrow indicates the northwesterly direction of the low-level wind at the ship that is consistent with the radial velocity field. (b)  $0.8^\circ$  elevation angle scan of reflectivity for the region of radar data in (a). A NW-SE azimuth line starting at the radar is shown. The ship is at the NW end of the line. (c) Vertical cross section of radar reflectivity (dBZ) along the SW-NE azimuth in (b). (d) Vertical cross section of radial velocity along the SW-NE azimuth in (b).

*b. Meridional component of midlevel inflow into super convective systems located in the strong westerly region of the Kelvin-Rossby wave*

The super convective systems in the southwestern quadrant of the northern gyre of the Kelvin-Rossby wave observed on 22–27 December (Fig. 3) exhibited an acceleration of midlevel inflow as a mesoscale system matured. Figure 22 illustrates this acceleration by showing a sequence of radial velocity patterns at the 4.5-km level. The dark blue colors indicate the maximum radial wind direction toward the ship (center of each panel), and the yellow colors show the maximum radial wind directed away from the ship. The pattern of colors indicate a general direction of the flow across the ship from northwest to southeast. During the 4-h period shown, strength of the northwesterly wind increased in magnitude by several meters per second. Looking at the

patterns in more detail, one sees a dark blue patch of strong northerly component wind at the far north extremity of the field of view of the ship radar. As time progressed, this blue patch ( $\sim 12 \text{ m s}^{-1}$  magnitude) intensified to light purple ( $\sim 20 \text{ m s}^{-1}$  magnitude) and moved southward over the ship. By 1352 UTC, the northwesterly flow just south of the ship had increased by about  $10 \text{ m s}^{-1}$  compared to 4 h earlier (as seen by the colors brightening from brown to bright gold). The intensified northerly component of flow was evidently felt also at low levels. Figure 23a shows an east-west line of cells that formed just to the south of the area of Doppler radial winds shown by the *Vickers* radar in Fig. 22. Apparently, the northerly component of momentum transported downward by the midlevel inflow jet gave the low-level gust front winds a northerly component, and the pattern of formation of new convective cells

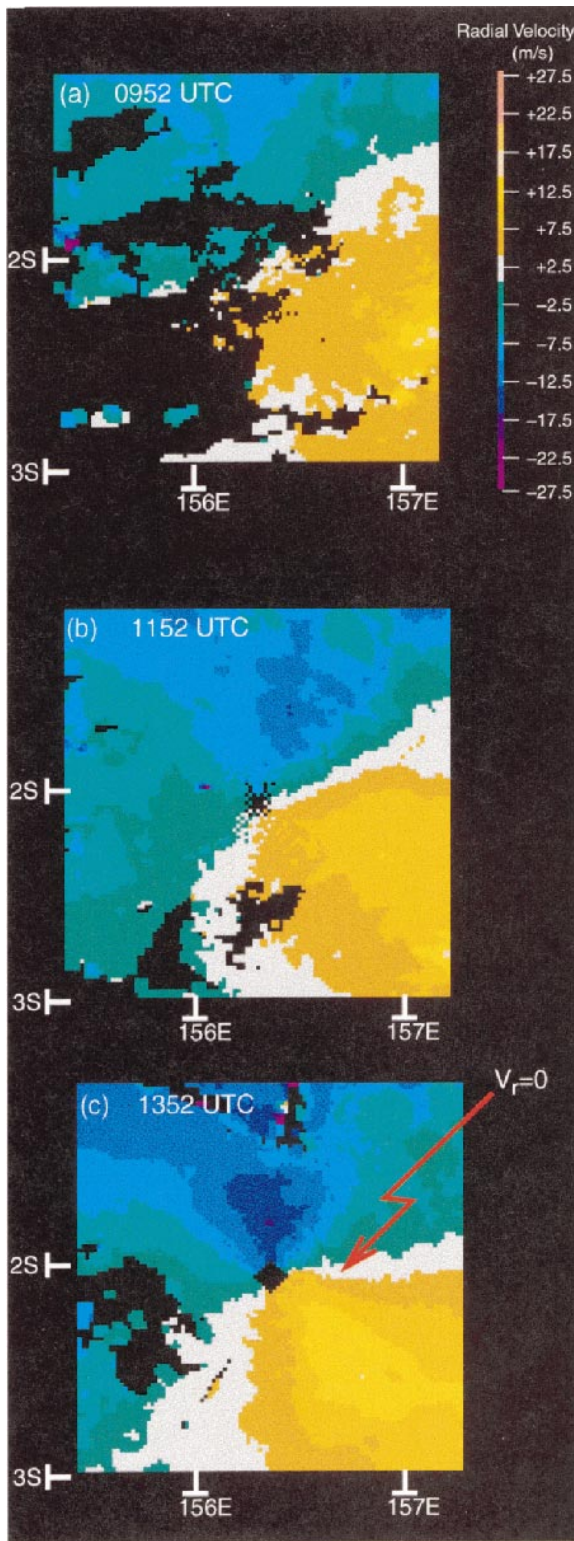


FIG. 22. Sequence of Doppler radar radial velocity ( $\text{m s}^{-1}$ ) at the 4.5-km level obtained on 22 Dec 1992 with the radar on the *Vickers*. The zero radial velocity line [marked by arrow in (c)] passes through the ship position at the center of the figure.

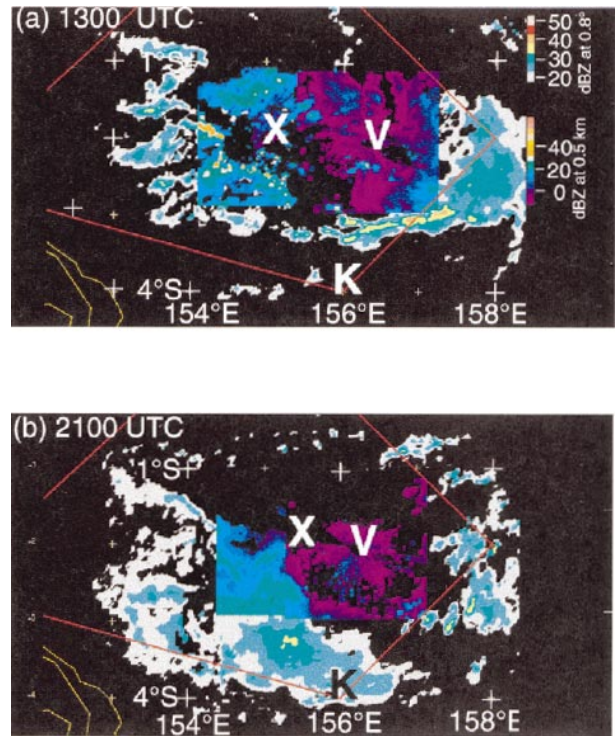


FIG. 23. Composite of 22 Dec 1992 radar reflectivity from ships *Xiangyanghong #5* (X) and *Vickers* (V). The *Vickers* data are plotted over the #5 data. The data in a 200-km square region surrounding each ship are the Cartesian interpolated data for the 0.5-km level. (For the *Vickers*, this is the same horizontal region shown in Fig. 22.) The data outside of the 200-km square regions are the noninterpolated data for the lowest elevation angle ( $0.8^\circ$ ), which shows the echo out to the farthest range seen by the radar. These outer data are too far from the radar to be quantitative but they give a good qualitative impression of the echo farther from the radar. Trapezoid is the boundary of the TOGA COARE IFA. The southernmost point of the IFA, (point K at  $4^\circ\text{S}$ ,  $156^\circ\text{E}$ ) was the location of the ship R/V *Kexue #1* referred to in Fig. 24.

changed from the eastern to the southern side of the precipitation area.

The east–west line developing to the south of the ships (Fig. 23a) moved southward and evolved into a large stratiform precipitation region. This stratiform region was over the ship R/V *Kexue #1* (point K in Figs. 23a,b) from about 1700 to 2100 UTC. The time series of surface data on the ship (not shown) also showed the surface wind becoming northwesterly during this time period. The wind profiler on the *Kexue #1* showed that the surface northwesterlies occurred as the northwesterly midlevel flow into the super convective systems dipped down to the surface in concert with the passage of the mesoscale stratiform region over the ship (Fig. 24; 1700–2100 UTC). The profiler thus provides corroboration of the momentum transport by the midlevel inflow into the super convective system by an instrument other than the Doppler precipitation radars.

Referring back to Fig. 3 we see that the late December super convective systems were on the northern side of

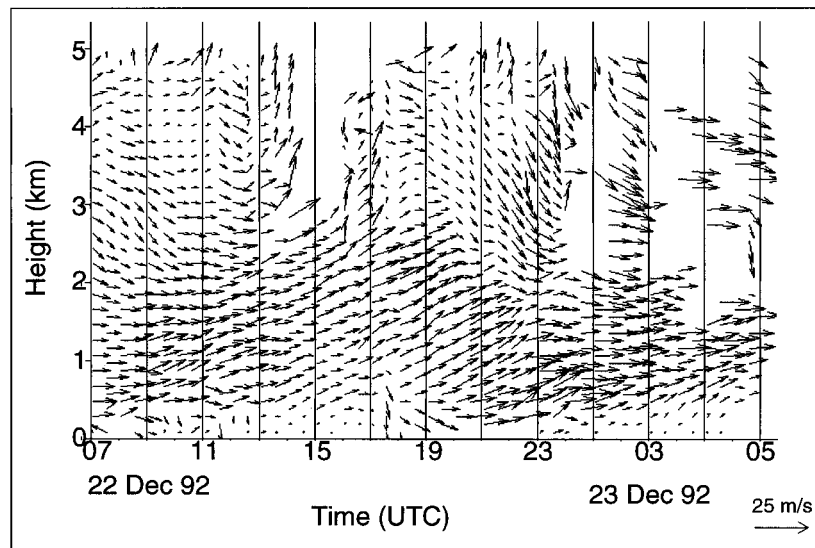


FIG. 24. Wind data from the ship R/V *Kexue #1* (point K in Fig. 23) taken with a 915-MHz profiler during the time period shown in Fig. 23.

the axis of strong westerlies between the large-scale Rossby gyres. We speculate that a super convective system south of this axis would have midlevel inflows transporting southerly momentum downward. The momentum transports by the super convective systems thus would seem to favor new convective generation in the axis of the strong westerlies. Such favoring in the core of the westerly jet would constitute another positive feedback to the westerlies, as it would act to concentrate the future convective heating and momentum transports in the heart of the westerlies.

*c. Smaller convective systems located in the strong westerly region of the Kelvin–Rossby wave*

The cloud systems we have examined in detail above for both the westerly onset and strong westerly regions of the large-scale Kelvin–Rossby wave system were the very large super convective systems. Smaller mesoscale convective systems are more common but generally receive less attention in the literature. The TOGA COARE storms observed by airborne and shipborne Doppler radar on 9, 10, and 18 February 1993 were of the smaller type (open symbols in Fig. 3).

Two storms were observed on 9 February. The first was observed in the IFA by shipborne dual-Doppler radar (Peterson et al. 1999). In its early stage it was perpendicular to the low-level shear and parallel to the midlevel shear. As the system matured, momentum transport by the system eliminated the low-level shear while having little effect on the midlevel shear. This storm was of the “shear-parallel” type studied previously by Tao and Soong (1986) and Dudhia and Moncrieff (1987). Another shear-parallel line on the same day but some 400 km to the southeast of the IFA storm

was documented by airborne multiple airborne Doppler radars and investigated by Hildebrand et al. (1996) and Roux (1998). The 18 February storm analyzed by Hildebrand (1998) was a third example of a shear-parallel convective system in the region of westerlies of the Kelvin–Rossby wave, though it occurred toward the west end of the westerly core, just before the transition to easterlies. These three shear-parallel cases were similar in that the primary overturning was local to the storm and primarily transverse to the large-scale shear vector [Fig. 5 of Peterson et al. (1999); Fig. 7a of Hildebrand et al. (1996)]. These cross-shear circulations appear to have been local to the mesoscale system. The downward branch of these circulations began at middle levels and sloped down under the updraft and appear to be generated within the convective system.

Smull and Houze (1987) suggested that the midlevel rear inflow of squall lines is usually internally generated by the convective and mesoscale pressure field within the storm, and the relative speed of the midlevel rear inflow at the back edge of the storm is usually weak. They found further, though, that in rare cases the rear inflow was very strong across the back edge, and in these cases the rear inflow was in large part forced by the large-scale environment relative flow across the back edge.

The downward circulations of the shear-parallel lines in TOGA COARE are evidently not as strongly forced by the large-scale environmental midlevel flow as are the midlevel inflows of the much larger super convective systems. The larger super convective systems appear to take on an organization in which the direction and speed of the midlevel inflow is strongly forced by the large-scale shear. In the TOGA COARE region, the large-scale shear is dominated by the zonal component of the

flow. The midlevel inflow set up by the large-scale shear is then enhanced by the latent cooling processes (sublimation, melting, and evaporation) under the widespread stratiform cloud. Thus, the super convective systems appear to be much more effective at transporting large quantities of zonal (along shear) momentum from midlevels down to low levels than the smaller shear-parallel mesoscale systems. In this sense they may be much stronger agents of interaction with the large-scale flow, as suggested by Moncrieff and Klinker (1997).

### 9. Momentum transports by the mesoscale midlevel inflow jets of super convective systems in contrasting regions of the Kelvin–Rossby wave

#### a. Factors determining the direction and magnitude of the mesoscale midlevel inflow jet

From the radar data analyses in sections 7 and 8 and the synoptic-scale wind field in the environment (e.g., Fig. 8), we infer that two important factors were involved in the formation of the mesoscale midlevel inflow jet of super convective systems in the Kelvin–Rossby wave:

- 1) The basic *direction* of the midlevel inflow to super convective systems was determined primarily by large-scale environment flow in midlevels. The midlevel zonal flow was oppositely directed in the westerly onset and strong westerly phases of the Kelvin–Rossby wave (Fig. 4). Midlevel air in the westerly onset region entered mesoscale systems with a strong easterly component. Midlevel air in the strong westerly phase of the Kelvin–Rossby wave entered mesoscale systems with a strong westerly component. Super convective systems therefore had midlevel easterly components in the westerly onset phase of the Kelvin–Rossby wave and westerly components in the strong westerly phase of the Kelvin–Rossby wave.
- 2) The *intensity* of the midlevel inflow to super convective systems was enhanced by the life cycle behavior of convection occurring within the systems. As individual convective elements went through their life cycles and filled the middle to upper levels of a mesoscale region with buoyant, ice particle-filled air, the cloud and precipitation structure of the mesoscale system matured and formed a mid- to upper-level stratiform deck. This contiguous feature made the midlevel inflow jet visible on radar. The convectively generated ice particles falling from the stratiform cloud deck subjected the entering ambient air below the sloping base to sublimation cooling. The midlevel inflow (easterly in the westerly onset phase and westerly in the strong westerly phase) probably accelerated in response to mesoscale low pressure produced by processes within the mesoscale cloud system and subsided in response to the sub-

limation cooling and melting processes under the stratiform deck. Thus, the midlevel inflow from the environment accelerated and sank as it extended across the super convective system. The ultimate breadth and duration of the mesoscale jet probably depended on the number of cells contributing to the mesoscale cloud system in space and over time. As pointed out by Yuter and Houze (1998) the size and lifetime of deep, broad stratiform cloud decks depend, among other things, on the ability of the ambient atmosphere to sustain a population of deep convective cells in a wide area for a long time. Upscale growth and sustainability of TOGA COARE super convective systems are in turn controlled by the vertically integrated moist-static energy of the lowest kilometer of the atmosphere (Kingsmill and Houze 1999b) and/or on having favorable environmental shear (Rotunno et al. 1988).

The jet subsided below the melting level, and a layer of convergence coincided with the melting layer. As the entering flow intensified and descended within the mesoscale system, horizontal pressure gradient forces within the system did not change the basic directional component of the midlevel flow, which remained easterly in systems located in the westerly onset phase and westerly in systems located in the strong westerly phase of the Kelvin–Rossby wave.

#### b. Momentum transport by super convective systems in the westerly onset region

In the westerly onset region of the TOGA COARE Kelvin–Rossby wave composite (Fig. 3), where the ambient midlevel inflow was from the east, the intensifying and subsiding midlevel circulation within the super convective systems transported easterly momentum to lower levels over large portions of the precipitation area from time to time (the regions of easterly component flow west of the ship in Figs. 13d,g).

When the easterly midlevel inflow was not coming down to the surface, new convective cells tended to form on the east side of the super convective system. In the right-hand box of Fig. 25, the arrows outside the precipitation area show the field of generally westerly ambient low-level wind characterizing the large-scale westerly onset region. The arrow labeled g1 represents the sense of the gust front wind typically triggering new cells; it was evidently greater than the ambient westerly component because the local convective scale hydrostatic pressure maximum under the rain shafts of existing cells would produce an enhancement of the westerly low-level wind on the east side of the system (as seen at the forward edge of the gust fronts in Figs. 14b, 15d, and 16c).

The heavy arrow in Fig. 25 indicates the midlevel ambient easterly wind entering the super convective system to form the midlevel inflow, which transported east-

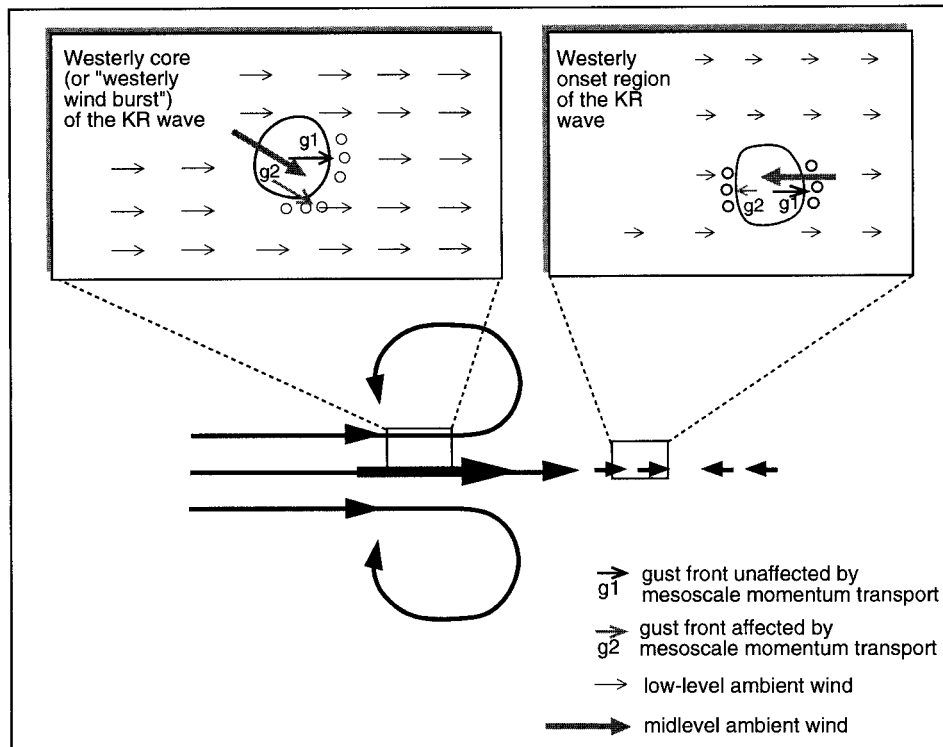


FIG. 25. Drawing illustrating our interpretation of the behavior of mesoscale convective systems observed by Doppler radar in two parts of the atmospheric Kelvin–Rossby wave as it occurred over the tropical Pacific warm pool during TOGA COARE. Streamlines indicate the wind direction at about the 850-mb level. The bold streamline indicates the core of strong westerlies (the “westerly wind burst”) in the Kelvin–Rossby wave. The contours within the boxes indicate the location of precipitation of a mesoscale convective system. The small circles indicate where new convection forms. The midlevel ambient wind is incorporated into the super convective system and is organized into a subsiding enhanced midlevel inflow jet transporting momentum to lower levels. This process reduces the large-scale mean low-level westerly momentum in the westerly onset zone and increases the westerlies in the strong westerly region of the wave. In the westerly onset region, the mesoscale momentum transport sometimes enhances the low-level easterly gust front and new cell formation on the western side of the super convective system. In the strong westerly region, acceleration of the northwesterly midlevel inflow in the later stages of the mesoscale convective system leads to northerly component gust fronts and cell formation on the southern side of the system.

erly momentum inward and downward. This transport constituted a negative momentum feedback, as it counteracted the low-level westerlies that were trying to become established in this portion of the Kelvin–Rossby wave. Whenever this easterly flow approached the surface, it produced an *easterly* component gust front wind, which reinforced gust convergence (also driven by convective dynamics) and favored triggering of new cells on the west side of the mesoscale system ( $g_2$  in the right-hand box of Fig. 25).

### c. Momentum transport by super convective systems in the strong westerly region

In the strong westerly phase of the Kelvin–Rossby wave, the midlevel inflow was produced by the same physical processes. The ambient flow determined the general direction of the midlevel flow entering the super convective systems, and the deep-convection-produced

layer of ice cloud, which precipitated into the inflow. This layer of precipitation made the midlevel inflow visible on radar. As the stratiform precipitation particles sublimated, melted, and evaporated, the latent cooling forced the air to subside. Midlevel mesolows internal to the cloud system probably also accelerated the midlevel inflow toward the interior of the super convective system. However, the different direction of the midlevel environmental wind led to the mesoscale inflow having a very different feedback effect on the mean large-scale flow. In the region sampled by ship radars (left-hand box in Fig. 25), the generally northwesterly ambient midlevel flow (heavy arrow) had a westerly component that was stronger than the  $u$  component of the ambient westerly flow at low levels. Thus, unlike in the westerly onset region of the Kelvin–Rossby wave, the downward transport of momentum by the midlevel westerly inflow of super convective systems in the low-level strong westerly region of the wave constituted a positive mo-

mentum feedback by strengthening the average low-level westerly momentum field in the region where the westerlies (constituting the “westerly wind burst”) were already a local maximum.

In the strong westerly region of the large-scale Kelvin–Rossby wind pattern indicated by the left-hand box of Fig. 25, the midlevel inflows of super convective systems also transported meridional momentum downward. Ship Doppler radar data indicated that as the December super convective systems matured, the north-westerly midlevel inflow increased in magnitude as the mesoscale system developed (Fig. 22). Northerly components of momentum transported downward by the midlevel inflow jet gave the low-level gust front winds a northerly component, which produced convergence and new cell development on the south side of the mesoscale convective system (Fig. 23). This process is indicated by vector  $g_2$  and a line of new cells to the south in the left-hand box of Fig. 25. We speculate that the mirror image of the left-hand box in Fig. 25 would be seen south of the equator. In this region the midlevel inflow would have been from the southwest, and new cells would have been favored on the north sides of super convective systems. Such favoring of triggering on the westerly jet side of the convective systems would constitute another positive feedback to the westerlies, as it would act to concentrate the future convective heating and momentum transports in the heart of the westerlies.

## 10. Conclusions

An important characteristic of TOGA COARE is that it systematically sampled convection over a whole season (November 1992–February 1993)—a sufficiently long period that the variation in the detailed structure of cloud systems observed by Doppler radar could be analyzed as a function of the slowly evolving large-scale dynamic environment, which in the TOGA COARE region was dominated from December through February by the near-equatorial atmospheric Kelvin–Rossby wave. This study differs from many traditional attempts to relate tropical convection to the large-scale “flow,” that is, to the large-scale wind, thermal, and moisture fields. Instead, we relate the convective structure to an identifiable large-scale *phenomenon*, namely, the Kelvin–Rossby wave, which was the proximate cause of the ambient large-scale fields. This approach opens the possibility of understanding the *process* interaction rather than approaching the problem as a “scale interaction.”

This study has focused on the largest cloud systems of the TOGA COARE region. Several “super convective systems” were documented by Doppler radars aboard aircraft and ships. The Doppler radial velocities measured by these radars indicate the characteristic internal circulations of the super convective systems. We have investigated super convective systems in two dis-

tinct locations with respect to the large-scale wave structure: the westerly onset and strong westerly regions of the Kelvin–Rossby wave. Mesoscale midlevel inflow develops under the widespread stratiform cloud deck of the mesoscale convective system. The direction of the midlevel inflow is determined by the large-scale flow. The midlevel inflow strengthens and is induced to sink under the precipitating stratiform deck. In the westerly onset region, the momentum feedback by this subsiding mesoscale midlevel inflow to the large-scale low-level Kelvin–Rossby wave winds is negative. It transports easterly momentum to low levels, where the wave is trying to establish a westerly flow on the large scale. In the strong westerly (“westerly wind burst”) region, the momentum feedback is positive, strengthening the already strong westerlies at low levels. This latter result is entirely consistent with the general circulation model results of Moncrieff and Klinker (1997).

The super convective systems also transport meridional momentum. The meridional component of the midlevel inflow, associated with the large-scale Rossby gyres lying on either side of the westerly wind maximum tend to produce redevelopment on the side of the system nearest the center of the westerly core, thus further strengthening and concentrating the low-level westerly core of the large-scale wave.

The direction of the midlevel inflow, and hence the sign of its mesoscale momentum transport, are determined by the large-scale ambient shear, a property of the Kelvin–Rossby wave phase. Thus, both the primary large-scale control and the feedback of the momentum transport of the super convective systems in the TOGA COARE regime appear to be functions of location with respect to the Kelvin–Rossby wave.

Within the same super convective system the *convective-scale* momentum feedbacks may be opposite in sign to the *mesoscale* feedbacks affected by the subsiding midlevel mesoscale inflows associated with the stratiform cloud deck. In addition, the convective-scale momentum transport may vary in sign from one part to another of the super convective system, regardless of where the super convective system is located with respect to the large-scale wave. This behavior was also noted by Moncrieff and Klinker (1997). The convective-scale momentum fluxes are thus not entirely systematic in any given part of the wave. In the westerly onset region, many of the convective-scale updrafts of super convective systems systematically transport easterly momentum upward, while the mesoscale inflow circulation, which develops in connection with the stratiform cloud deck, transports easterly momentum downward. This behavior points out the importance of predicting the right amount of stratiform cloud and precipitation development in evaluating momentum feedbacks to the large scale.

This study distinguishes the role of the super convective systems (the very largest systems) in the TOGA COARE regime from mesoscale convective systems of

a smaller scale. The super convective systems appear to be those that develop mesoscale circulations that overturn in the along-shear direction. The shear in the TOGA COARE regime is dominated by the zonal wind component. The subsiding midlevel inflows of super convective systems transport large quantities of zonal momentum downward—hence the negative feedback in the westerly onset region and the positive feedback in the strong westerly region of the Kelvin–Rossby wave. Studies of smaller mesoscale systems (Hildebrand et al. 1996; Hildebrand 1998; Roux 1998; Peterson et al. 1999) indicate that the convection tends to align parallel to the environmental shear vector and that the mesoscale overturning is predominantly transverse to the large-scale (mainly zonal) shear. A major difference between these smaller “shear-parallel” systems and the larger super convective systems appears to be the ability of the latter to transport the midlevel zonal winds down to low levels over areas of the scale of the large cloud shields and cold pools of these big systems. Since the large-scale wave dynamics is largely defined in terms of the zonal flow (manifested most dramatically by the westerly wind burst of the Kelvin–Rossby wave), it appears that the super convective systems may be a key link in the convective–large-scale interaction over the TOGA COARE region.

The two distinct types of momentum transport by the different large-scale flow regimes within the Kelvin–Rossby wave, which we have described in this paper, have possibly important implications for the large-scale evolution of the ISO over the western Pacific warm pool. First, the downward easterly momentum transport by the mesoscale midlevel inflows to super convective systems during the onset of the large-scale surface westerly phase contributes (along with convective dynamics) to the development of new convection on the west side of the old system through enhanced mesoscale low-level convergence. This tendency helps to explain why on the large scale the convection occurs preferentially in the large-scale westerlies. Second, this downward easterly momentum transport tends to slow down the eastward propagation of the ISO; this effect on the ISO might be called “super convective friction.” During the strong deep westerly phase of the Kelvin–Rossby wave, the downward westerly momentum transport by the super convective systems enhances the surface westerly, which also helps to explain the observed collocation of convection and surface westerlies.

This empirical study has pointed out some basic features of the convective–large-scale interaction in the tropical atmosphere over the warm pool. The dataset alone, however, can only address a limited number of issues. The results obtained here are now ready for examination in high-resolution modeling studies aimed at understanding the nature of the convective and mesoscale momentum feedbacks. High-resolution mesoscale models run over a large tropical oceanic domain can test the idea, suggested by our results, that the midlevel

inflow jet that forms in the stratiform regions of super convective systems produces a negative momentum feedback in the westerly onset region and a positive momentum feedback in the westerly wind burst region of the Kelvin–Rossby wave. The general circulation model results of Moncrieff and Klinker (1997) strongly suggest that further modeling studies will confirm our conclusions. Simulations with more detailed models will be demanding, as they will not only require high resolution and a large domain but also a robust ice-phase microphysical parameterization to simulate properly the inflow jet development. However, successful model reproduction of our momentum transport results will lead to further insights into the convective–large-scale interaction in the atmosphere.

*Acknowledgments.* The authors greatly appreciate the superb and laborious efforts of the flight crews and ship crews of the research aircraft and ships in TOGA COARE. Peter Hildebrand and Bradley Smull made extremely helpful comments during the writing and revising of the manuscript. Candace Gudmundson edited the manuscript and Kay Dewar edited the graphics. This research was supported by the following grants: National Science Foundation Grant ATM-9024431, JISAO Cooperative Agreements NA37RJ0198 and NA67R50155, TRMM NASA Grants NAG5-1599 and NAG5-4795, and EOS NASA Grants NAG5-6101 and NAGW-2633.

#### REFERENCES

- Betts, A. K., 1974: Thermodynamic classification of tropical convective soundings. *Mon. Wea. Rev.*, **102**, 760–764.
- Braun, S. A., and R. A. Houze Jr., 1997: The evolution of the 10–11 June 1985 PRE-STORM squall line: Initiation, development of rear inflow, and dissipation. *Mon. Wea. Rev.*, **125**, 478–504.
- Chang, C.-P., 1977: Viscous internal gravity waves and low-frequency oscillations in the Tropics. *J. Atmos. Sci.*, **34**, 901–910.
- Chen, S. S., and W. M. Frank, 1993: A numerical study of the genesis of extratropical convective mesovortices. Part I: Evolution and dynamics. *J. Atmos. Sci.*, **50**, 2401–2426.
- , and R. A. Houze Jr., 1997: Interannual variability of deep convection over the tropical warm pool. *J. Geophys. Res.*, **102**, 25 783–25 795.
- , —, and B. E. Mapes, 1996: Multiscale variability of deep convection in relation to large-scale circulation in TOGA COARE. *J. Atmos. Sci.*, **53**, 1380–1409.
- Chong, M., and O. Bousquet, 1999: A mesovortex within a near-equatorial mesoscale convective system during TOGA COARE. *Mon. Wea. Rev.*, **127**, 1145–1156.
- Corbet, J., C. Mueller, C. Burghart, K. Gould, and G. Granger, 1994: Zeb: Software for integration, display, and management of diverse environmental datasets. *Bull. Amer. Meteor. Soc.*, **75**, 783–792.
- Cressman, G. P., 1959: An operational objective analysis system. *Mon. Wea. Rev.*, **87**, 367–374.
- Dudhia, J., and M. W. Moncrieff, 1987: A numerical simulation of quasi-stationary tropical convective bands. *Quart. J. Roy. Meteor. Soc.*, **113**, 929–967.
- Fein, J. S., and J. P. Kuetner, 1980: Report on the summer MONEX field phase. *Bull. Amer. Meteor. Soc.*, **61**, 461–474.
- Fovell, R. G., and Y. Ogura, 1988: Numerical simulation of a mid-latitude squall line in two dimensions. *J. Atmos. Sci.*, **45**, 3846–3879.

- , and —, 1989: Effect of vertical wind shear on numerically simulated multicell storm structure. *J. Atmos. Sci.*, **46**, 3144–3176.
- Gill, A., 1980: Some simple solutions for heat-induced tropical circulation. *Quart. J. Roy. Meteor. Soc.*, **106**, 447–462.
- Godfrey, J. S., R. A. Houze Jr., R. H. Johnson, R. Lukas, J.-L. Redelsperger, A. Sumi, and R. Weller, 1998: COARE: An interim report. *J. Geophys. Res.*, **103** (7), 14 395–14 450.
- Greenfield, R. S., and T. N. Krishnamurti, 1979: The Winter Monsoon Experiment—Report of December 1978 field phase. *Bull. Amer. Meteor. Soc.*, **60**, 439–444.
- Halverson, J. B., B. S. Ferrier, T. M. Rickenbach, J. Simpson, and W.-K. Tao, 1999: An ensemble of convective systems on 11 February 1993 during TOGA COARE: Morphology, rainfall characteristics, and anvil cloud interactions. *Mon. Wea. Rev.*, **127**, 1208–1228.
- Hartmann, D. L., H. H. Hendon, and R. A. Houze Jr., 1984: Some implications of the mesoscale circulations in tropical cloud clusters for large-scale dynamics and climate. *J. Atmos. Sci.*, **41**, 113–121.
- Hendon, H. H., and B. Liebmann, 1994: Organization of convection within the Madden-Julian oscillation. *J. Geophys. Res.*, **99**, 8073–8083.
- , and M. L. Salby, 1994: The life cycle of the Madden-Julian oscillation. *J. Atmos. Sci.*, **51**, 2225–2237.
- Hildebrand, P. H., 1998: Shear-parallel moist convection over the tropical ocean: A case study from 18 February 1993 TOGA COARE. *Mon. Wea. Rev.*, **126**, 1952–1976.
- , W.-C. Lee, C. A. Walther, C. Frush, M. Randall, E. Loew, R. Neitzel, and R. Parsons, 1996: Airborne Doppler weather radar: High-resolution observations from TOGA COARE. *Bull. Amer. Meteor. Soc.*, **77**, 213–232.
- Holland, G. J., J. L. McBride, R. K. Smith, D. Jasper, and T. D. Keenan, 1986: The BMRC Australian Monsoon Experiment: AMEX. *Bull. Amer. Meteor. Soc.*, **67**, 1466–1472.
- Houze, R. A., Jr., 1982: Cloud clusters and large-scale vertical motions in the Tropics. *J. Meteor. Soc. Japan*, **60**, 396–410.
- , 1989: Observed structure of mesoscale convective systems and implications for large-scale heating. *Quart. J. Roy. Meteor. Soc.*, **115**, 425–461.
- , 1993: *Cloud Dynamics*. Academic Press, 573 pp.
- , 1997: Stratiform precipitation in regions of convection: A meteorological paradox? *Bull. Amer. Meteor. Soc.*, **78**, 2179–2196.
- , S. A. Rutledge, M. I. Biggerstaff, and B. F. Smull, 1989: Interpretation of Doppler weather radar displays of midlatitude mesoscale convective systems. *Bull. Amer. Meteor. Soc.*, **70**, 608–619.
- , B. F. Smull, and P. Dodge, 1990: Mesoscale organization of springtime rainstorms in Oklahoma. *Mon. Wea. Rev.*, **118**, 613–654.
- Johnson, R. H., and X. Lin, 1997: Episodic trade wind regimes over the western Pacific warm pool. *J. Atmos. Sci.*, **54**, 2020–2034.
- Jorgensen, D. P., T. Matejka, and J. D. DuGranrut, 1996: Multi-beam techniques for deriving wind fields from airborne Doppler radars. *Meteor. Atmos. Phys.*, **59**, 83–104.
- , M. A. LeMone, and S. B. Trier, 1997: Structure and evolution of the 22 February 1993 TOGA COARE squall line: Aircraft observations of precipitation, circulation, and surface energy fluxes. *J. Atmos. Sci.*, **54**, 1961–1985.
- Kingsmill, D. E., and R. A. Houze Jr., 1999a: Kinematic characteristics of air flowing into and out of precipitating convection over the west Pacific warm pool: An airborne Doppler radar survey. *Quart. J. Roy. Meteor. Soc.*, **125**, 1165–1207.
- , and —, 1999b: Thermodynamic characteristics of precipitating convection over the west Pacific warm pool. *Quart. J. Roy. Meteor. Soc.*, **125**, 1209–1229.
- Kuettner, J. P., and D. E. Parker, 1976: GATE: Report on the field phase. *Bull. Amer. Meteor. Soc.*, **57**, 11–27.
- Lau, K.-M., L. Peng, C. H. Sui, and T. Nakazawa, 1989: Dynamics of super cloud clusters, westerly wind bursts, 30–60 day oscillations and ENSO: A unified view. *J. Meteor. Soc. Japan*, **67**, 205–219.
- LeMone, M. A., 1983: Momentum transport by a line of cumulonimbus. *J. Atmos. Sci.*, **40**, 1815–1834.
- Lewis, S. A., M. A. LeMone, and D. P. Jorgensen, 1998: Evolution and dynamics of a late-stage squall line that occurred on 20 February 1993 during TOGA COARE. *Mon. Wea. Rev.*, **126**, 3189–3212.
- Lin, X., and R. H. Johnson, 1996: Kinematic and thermodynamic characteristics of the flow over the western Pacific warm pool during TOGA COARE. *J. Atmos. Sci.*, **53**, 695–715.
- Madden, R., and P. Julian, 1971: Detection of a 40–50 day oscillation in the zonal wind in the tropical Pacific. *J. Atmos. Sci.*, **28**, 702–708.
- , and —, 1972: Description of global scale circulation cells in the Tropics with a 40–50 day period. *J. Atmos. Sci.*, **29**, 1109–1123.
- , and —, 1994: Observations of the 40–50 day tropical oscillation—A review. *Mon. Wea. Rev.*, **122**, 814–837.
- Mapes, B. E., and R. A. Houze Jr., 1992: An integrated view of the 1987 Australian monsoon and its mesoscale convective systems. Part I: Horizontal structure. *Quart. J. Roy. Meteor. Soc.*, **118**, 927–963.
- , and —, 1993a: An integrated view of the 1987 Australian monsoon and its mesoscale convective systems. Part II: Vertical structure. *Quart. J. Roy. Meteor. Soc.*, **119**, 733–754.
- , and —, 1993b: Cloud clusters and superclusters over the oceanic warm pool. *Mon. Wea. Rev.*, **121**, 1398–1415.
- , and —, 1995: Diabatic divergence profiles in western Pacific mesoscale convective systems. *J. Atmos. Sci.*, **52**, 1807–1828.
- , and P. Zuidema, 1996: Radiative-dynamical consequences of dry tongues in the tropical atmosphere. *J. Atmos. Sci.*, **53**, 620–638.
- Mohr, C. G., L. J. Miller, R. L. Vaughan, and H. W. Frank, 1986: The merger of mesoscale datasets into a common Cartesian format for efficient and systematic analyses. *J. Atmos. Oceanic Technol.*, **3**, 143–161.
- Moncrieff, M. W., and E. Klinker, 1997: Organized convective systems in the tropical western Pacific as a process in general circulation models: A TOGA COARE case study. *Quart. J. Roy. Meteor. Soc.*, **123**, 805–827.
- Nakazawa, T., 1988: Tropical super clusters within intraseasonal variations over the western Pacific. *J. Meteor. Soc. Japan*, **66**, 823–839.
- Oye, R., and R. Carbone, 1981: Interactive Doppler editing software. Preprints, *20th Conf. on Radar Meteorology*, Boston, MA, Amer. Meteor. Soc., 683–689.
- , C. Mueller, and S. Smith, 1995: Software for radar translation, visualization, editing, and interpolation. Preprints, *27th Conf. on Radar Meteorology*, Vail, CO, Amer. Meteor. Soc., 359–361.
- Peterson, W. A., R. C. Cifelli, S. A. Rutledge, B. S. Ferrier, and B. F. Smull, 1999: Shipborne dual-Doppler operations during TOGA COARE: Integrated observations of storm kinematics and electrification. *Bull. Amer. Meteor. Soc.*, **80**, 81–97.
- Raymond, D. J., 1995: Regulation of moist convection over the west Pacific warm pool. *J. Atmos. Sci.*, **52**, 3945–3959.
- Rotunno, R., J. B. Klemp, and M. L. Weisman, 1988: A theory for strong, long-lived squall lines. *J. Atmos. Sci.*, **45**, 463–485.
- Roux, F., 1998: The oceanic mesoscale convective system observed with airborne Doppler radars on 9 February 1993 during TOGA COARE: Structure, evolution and budgets. *Quart. J. Roy. Meteor. Soc.*, **124**, 585–614.
- Salby, M. L., 1996: *Fundamentals of Atmospheric Physics*. Academic Press, 627 pp.
- Short, D. A., P. A. Kucera, B. S. Ferrier, J. C. Gerlach, S. A. Rutledge, and O. W. Thiele, 1997: Shipboard radar rainfall patterns within the TOGA COARE IFA. *Bull. Amer. Meteor. Soc.*, **78**, 2817–2836.
- Skamarock, W. C., M. L. Weisman, and J. B. Klemp, 1994: Three-

- dimensional evolution of simulated long-lived squall lines. *J. Atmos. Sci.*, **51**, 2563–2584.
- Smull, B. F., and R. A. Houze Jr., 1987: Rear inflow in squall lines with trailing stratiform precipitation. *Mon. Wea. Rev.*, **115**, 2128–2148.
- Tao, W.-K., and S.-T. Soong, 1986: A study of the response of deep tropical clouds to mesoscale processes: Three-dimensional numerical experiments. *J. Atmos. Sci.*, **43**, 39–62.
- Wang, B., 1988: Dynamics of the tropical low-frequency waves: An analysis of the moist Kelvin wave. *J. Atmos. Sci.*, **45**, 2051–2065.
- Webster, P. J., 1972: Response of the tropical atmosphere to local, steady forcing. *Mon. Wea. Rev.*, **100**, 518–540.
- , 1973: Temporal variation of low-latitude circulations. *Mon. Wea. Rev.*, **101**, 803–816.
- , 1994: The role of hydrological processes in ocean–atmosphere interactions. *Rev. Geophys.*, **32**, 427–476.
- , and G. L. Stephens, 1980: Tropical upper-tropospheric extended clouds: Inferences from Winter MONEX. *J. Atmos. Sci.*, **37**, 1521–1541.
- , and R. A. Houze Jr., 1991: The Equatorial Mesoscale Experiment (EMEX): An overview. *Bull. Amer. Meteor. Soc.*, **72**, 1481–1505.
- Weisman, M. L., and J. B. Klemp, 1984: The structure and classification of numerically simulated convective storms in directionally varying wind shears. *Mon. Wea. Rev.*, **112**, 2479–2498.
- , and —, 1986: Characteristics of isolated convective storms. *Mesoscale Meteorology and Forecasting*, P. S. Ray, Ed., Amer. Meteor. Soc., 331–358.
- , —, and R. Rotunno, 1988: The structure and evolution of numerically simulated squall lines. *J. Atmos. Sci.*, **45**, 1990–2013.
- Weller, R. A., and S. P. Anderson, 1996: Surface meteorology and air–sea fluxes in the western equatorial Pacific warm pool during the TOGA Coupled Ocean–Atmosphere Response Experiment. *J. Climate*, **9**, 1959–1990.
- Xu, K.-M., and K. A. Emanuel, 1989: Is the tropical atmosphere conditionally unstable? *Mon. Wea. Rev.*, **117**, 1471–1479.
- Yang, M.-J., and R. A. Houze Jr., 1995: Sensitivity of squall-line rear inflow to ice microphysics and environmental humidity. *Mon. Wea. Rev.*, **123**, 3175–3193.
- Yuter, S. E., and R. A. Houze Jr., 1995: Three-dimensional kinematic and microphysical evolution of Florida cumulonimbus. Part III: Vertical mass transport, mass divergence, and synthesis. *Mon. Wea. Rev.*, **123**, 1964–1983.
- , and —, 1997: Measurements of raindrop size distributions over the Pacific warm pool and implications for Z–R relations. *J. Appl. Meteor.*, **36**, 847–867.
- , and —, 1998: The natural variability of precipitating clouds over the western Pacific warm pool. *Quart. J. Roy. Meteor. Soc.*, **124**, 53–99.
- , and —, 2000: The 1997 Pan American Climate Studies Tropical Eastern Pacific Process Study. Part I: ITCZ region. *Bull. Amer. Meteor. Soc.*, **81**, 451–481.
- , —, B. F. Smull, F. D. Marks Jr., J. R. Daugherty, and S. R. Brodzik, 1995: TOGA COARE aircraft mission summary images: An electronic atlas. *Bull. Amer. Meteor. Soc.*, **76**, 319–328.
- , Y. L. Serra, and R. A. Houze Jr., 2000: The 1997 Pan American Climate Studies Tropical Eastern Pacific Process Study. Part II: Stratocumulus region. *Bull. Amer. Meteor. Soc.*, **81**, 483–490.
- Zhang, D.-L., and J. M. Fritsch, 1987: Numerical simulation of the meso- $\beta$  scale structure and evolution of the 1977 Johnstown flood. Part II: Inertially stable warm-core vortex and the mesoscale convective complex. *J. Atmos. Sci.*, **44**, 2593–2612.
- , and —, 1988a: Numerical sensitivity experiments of varying model physics on the structure, evolution, and dynamics of two mesoscale convective systems. *J. Atmos. Sci.*, **45**, 261–293.
- , and —, 1988b: Numerical simulation of the meso- $\beta$  scale structure and evolution of the 1977 Johnstown flood. Part III: Internal gravity waves and the squall line. *J. Atmos. Sci.*, **45**, 1252–1268.
- , and K. Gao, 1989: Numerical simulation of an intense squall line during 10–11 June 1985 PRE-STORM. Part II: Rear inflow, surface pressure perturbations and stratiform precipitation. *Mon. Wea. Rev.*, **117**, 2067–2094.
- Zipser, E. J., 1969: The role of organized unsaturated convective downdrafts in the structure and rapid decay of an equatorial disturbance. *J. Appl. Meteor.*, **8**, 799–814.